Tumoral and stromal hMENA isoforms impact tertiary lymphoid structure localization in lung cancer and predict immune checkpoint blockade response in patients with cancer

Francesca Di Modugno,[a,**] Anna Di Carlo,[a] Sheila Spada,[a] Belinda Palermo,[a] Lorenzo D'Ambrosio,[a] Daniel D'Andrea,[b] Gaia Morello,[c] Beatrice Belmonte,[c] Isabella Sperduti,[d] Vittoria Balzano,[a] Enzo Gallo,[e] Roberta Melchionna,[a] Mariangela Panetta,[a] Giulia Campo,[a] Francesca De Nicola,[f] Frauke Goeman,[f] Barbara Antoniani,[e] Silvia Carpano,[g] Gianmaria Frigè,[h] Sarah Warren,[i] Filippo Gallina,[j] Diether Lambrechts,[k] Jieyi Xiong,[k] Benjamin G. Vincent,[l] Nathan Wheeler,[l] Dante S. Bortone,[l] Federico Cappuzzo,[g] Francesco Facciolo,[j] Claudio Tripodo,[c] Paolo Visca,[e] and Paola Nisticò[a,*]

[a]Tumor Immunology and Immunotherapy Unit, IRCCS-Regina Elena National Cancer Institute, Via E. Chianesi 53, 00144, Rome, Italy
[b]Department of Biosciences, School of Science and Technology, Nottingham Trent University, New Hall Block - Room 171, Clifton Campus - NG11 8NS, Nottingham, United Kingdom
[c]Tumor Immunology Unit, Department of Health Sciences, University of Palermo, Corso Tukory 211, 90134, Palermo, Italy
[d]Biostatistics and Scientific Direction, IRCCS-Regina Elena National Cancer Institute, Via E. Chianesi 53, 00144, Rome, Italy
[e]Pathology Unit, IRCCS-Regina Elena National Cancer Institute, Via E. Chianesi 53, 00144, Rome, Italy
[f]SAFU Unit, IRCCS-Regina Elena National Cancer Institute, Via E. Chianesi 53, 00144, Rome, Italy
[g]Second Division of Medical Oncology, IRCCS-Regina Elena National Cancer Institute, Via E. Chianesi 53, 00144, Rome, Italy
[h]Department of Experimental Oncology, IEO, European Institute of Oncology IRCCS, Via Ripamonti 435, Milan, Italy
[i]NanoString Technologies Inc., 530 Fairview Ave N, Seattle, WA, 98109, USA
[j]Thoracic-Surgery Unit, IRCCS-Regina Elena National Cancer Institute, Via E. Chianesi 53, 00144 Rome, Italy
[k]Center for Cancer Biology, Herestraat 49 box 912, VIB, 3000, Leuven, Belgium
[l]Lineberger Comprehensive Cancer Center, University of North Carolina at Chapel Hill, 5206 Marsico Hall, Chapel Hill, NC, 27599, USA

Summary

Background Tertiary Lymphoid Structures (TLS) correlate with positive outcomes in patients with NSCLC and the efficacy of immune checkpoint blockade (ICB) in cancer. The actin regulatory protein hMENA undergoes tissue-specific splicing, producing the epithelial hMENA[11a] linked to favorable prognosis in early NSCLC, and the mesenchymal hMENAΔv6 found in invasive cancer cells and pro-tumoral cancer-associated fibroblasts (CAFs). This study investigates how hMENA isoforms in tumor cells and CAFs relate to TLS presence, localization and impact on patient outcomes and ICB response.

Methods Methods involved RNA-SEQ on NSCLC cells with depleted hMENA isoforms. A retrospective observational study assessed tissues from surgically treated N0 patients with NSCLC, using immunohistochemistry for tumoral and stromal hMENA isoforms, fibronectin, and TLS presence. ICB-treated patient tumors were analyzed using Nanostring nCounter and GeoMx spatial transcriptomics. Multiparametric flow cytometry characterized B cells and tissue-resident memory T cells (T_{RM}). Survival and ICB response were estimated in the cohort and validated using bioinformatics pipelines in different datasets.

Findings Findings indicate that hMENA[11a] in NSCLC cells upregulates the TLS regulator LTβR, decreases fibronectin, and favors CXCL13 production by T_{RM}. Conversely, hMENAΔv6 in CAFs inhibits LTβR-related NF-kB pathway, reduces CXCL13 secretion, and promotes fibronectin production. These patterns are validated in N0 NSCLC tumors, where hMENA11a[high] expression, CAF hMENAΔv6[low], and stromal fibronectin[low] are associated with intratumoral TLS, linked to memory B cells and predictive of longer survival. The hMENA isoform pattern, fibronectin, and LTβR expression broadly predict ICB response in tumors where TLS indicates an anti-tumor immune response.

Interpretation This study uncovers hMENA alternative splicing as an unexplored contributor to TLS-related Tumor Immune Microenvironment (TIME) and a promising biomarker for clinical outcomes and likely ICB responsiveness in N0 patients with NSCLC.

*Corresponding author.
**Corresponding author.
    E-mail addresses: paola.nistico@ifo.it (P. Nisticò), francesca.dimodugno@ifo.it (F. Di Modugno).

Keywords: Tumor microenvironment; Tertiary lymphoid structures; Cancer-associated fibroblasts; Immune checkpoint blockade; Resistance to immunotherapy; Epithelial mesenchymal transition; Fibronectin; Non-small cell lung cancer; hMENA isoforms

Research in context

Evidence before this study
Tertiary lymphoid structures are crucial for an effective anti-tumor immune response and TLS gene signature are predictive of improved outcomes in patients treated with ICB. However, the determinants of TLS organization and localization in solid tumors are still unknown. The actin regulatory protein hMENA has been described as the only protein able to link adhesome to the nuclear envelope and able to regulate immune-related genes and fibronectin. Our previous data indicate that tissue-specific splicing program of hMENA generates two isoforms with opposite roles in the convergence of different epithelial to mesenchymal transition (EMT) related signaling pathways. The epithelial-associated hMENA[11a] isoform was a predictor of a longer survival of early node-negative NSCLC tissues, whereas the mesenchymal hMENAΔv6 is expressed in CAFs with pro-tumoral function, but its role as prognostic factor has not been still proved.

Added value of this study
Our findings reveal that the alternative splicing of actin cytoskeleton regulator hMENA impacts mechanisms underlying the communication among tumor cells, extracellular matrix, CAFs and T and B cells and is related to TLS localization and clinical outcome in N0 patients with NSCLC. The application of different computational tools able to detect splice variants highlighted hMENA isoforms as a predictor of response to ICB in tumors where TLS presence is related to an anti-tumor immune response.

Implications of all the available evidence
Herein, we provide evidence that the pattern of hMENA isoform expression in tumor cells and CAFs is a promising prognostic biomarker that may support the clinical decision for early-node negative patients with NSCLC, whose clinical management is still debated. Notably, we also provide a signature which includes hMENA isoforms, fibronectin and LTβR that may be predictive of response in patients treated with ICB. Further studies aimed at identifying drugs that may regulate hMENA isoform expression may pave the way for novel combined therapy.

Introduction

The identification of criteria for clinical management of early patients with non-small cell lung cancer (NSCLC) with lymph node negative tumors is still a big challenge.[1] The increased understanding of the crucial role of immune system in cancer and the advent of immunotherapy in the clinical practice have highlighted the impact of the tumor immune microenvironment (TIME) as source of prognostic and predictive information.[2] The immune checkpoint blockade (ICB) represents an unprecedented effective treatment, but yet, not all patients benefit, demanding the identification of mechanisms underlying the patient poor response.[3,4] Although tumor infiltrating cytotoxic T cells have been reported as associated with improved patient survival,[5] B cells localized in the tertiary lymphoid structures (TLS) are emerging as prognostic[6,7] and predictive biomarkers for tailoring immunotherapy in different cancer.[8–10] In patients with NSCLC the intratumoral enrichment of the plasma cell signature associated with the presence of TLS correlates with a clinical benefit from Programmed death-ligand 1 (PD-L1) checkpoint blockade.[11] Notably, plasma cells producing antibodies that bind to cancer cells and sustain the response to ICB disseminate into the tumor along tracks of peculiar fibroblasts.[12]

Different functions and subpopulation of cancer-associated fibroblasts (CAFs) immune permissive or immune suppressive have been identified at single cell level, such as CAFs negative for Fibroblast Activation Protein alpha (FAP) which produce C-X-C Motif Chemokine Ligand 13 (CXCL13) and mediate TLS development,[13] or immune suppressive extracellular matrix myofibroblast CAF (ECM-myCAF), producing high extracellular matrix (ECM) amount.[14] In lung adenocarcinoma (ADC) myofibroblasts have been correlated with poor overall survival (OS) rates.[15] Most NSCLC tumors are characterized by a fibrotic component with CAFs secreting ECM and producing soluble factors that support cancer progression and may hinder or prevent T-cell infiltration,[16–18] modulating immune cell activity.[19] Although CAFs are the major producers of the ECM, the impact of the ECM profile on the anti-tumor immunity still remains elusive, even if recent data have

highlighted its role as major contributor in immune cell exclusion and in turn poor patient outcome.[17,20]

Actin cytoskeleton organization and integrin signaling in tumor cells and in CAFs regulate ECM composition and mesenchymal traits, that have emerged as a common feature of different signatures of resistance to ICB.[21] The actin cytoskeleton regulatory protein hMENA (*ENAH* gene) undergoes tissue-specific splicing program with hMENA[11a] the "epithelial" isoform, and hMENAΔv6 the "mesenchymal" isoform, playing opposite roles in the convergence of different epithelial to mesenchymal transition (EMT) related signaling pathways,[22] including Transforming growth factor-β (TGFβ).[23] We have reported that the two hMENA isoforms differently affects the β1 integrin-ECM signaling pathways and that high hMENA[11a] and low stromal fibronectin could predict a favorable outcome of early-node-negative patients with NSCLC.[24] Recently, hMENA has been implicated in the regulation of actin-nuclear lamina interaction, chromatin organization and expression of several genes including Fibronectin 1 gene (FN1).[25] Importantly, we have also identified a crucial role of the mesenchymal hMENA/hMENAΔv6 isoforms expressed in CAFs, in regulating the bi-directional communication between CAFs and tumor cells.[26] Notably, *hMENA* is highly expressed in the subtype of immunosuppressive ECM-myCAF.[14]

Herein, we demonstrated that in NSCLC cell lines hMENA[11a] induces the expression of the TLS regulator Lymphotoxin β receptor (LTβR), whereas reduces the FN1 expression. Conversely, in CAFs hMENA/hMENAΔv6 favor FN1 expression and fibrillogenesis and inhibit LTβR expression, its downstream activation signal and the secretion of CXCL13, a relevant cytokine in TLS formation.[27] In the TIME CXCL13 is mainly produced by T_{RM} cells[28] and we found that in tumor cells the depletion of the hMENA[11a] isoform affects CXCL13 production by T_{RM} cells. That the tumor- and stroma-pattern of hMENA isoform associates with TLS localization and survival in early node-negative patients with NSCLC offers new insight in the controversial clinical management of these patients. Notably, we highlight that a signature that includes the hMENA pattern of expression, possesses a broad ability to predict response to ICB therapy in NSCLC, melanoma and triple-negative breast cancer (TNBC), as shown in different cohorts analyzed by different technologies.

Methods

Patient population and tissues specimens

The 94 patients with NSCLC without pathological lymph-node involvement (N0) analyzed for TLS presence and localization were resected with curative intent at the Regina Elena National Cancer Institute between 2001 and 2006. Patients' characteristics including age and sex and follow-up data were obtained in accordance with hospital charts and by corresponding with the referring physicians, analyzed, and reported according to Shuster et al.[29] The 8 patients analyzed for B cell characterization and the 8 patients for Tumor-infiltrating lymphocytes (TIL) CXCL13 expression, were resected with curative intent at the Regina Elena National Cancer Institute between 2018 and 2020. Sex identification was self-reported by study participants and eligible patients were all recruited without restriction on sex. Patients donated, after written informed consent, a portion of surgically resected tissue (for TIL isolation) and a time-matched blood sample (for peripheral blood mononuclear cell (PBMC) isolation). PBMC were isolated by the use of Ficoll-paque separation (Cedarlane's Lympholyte Cell Separation, Euroclone). Freshly resected lung tumors and adjacent lung tissues were processed within 20 min of removal from patient. Tissue samples were mechanically dissociated as small as possible under sterile conditions, and placed in incubator at 37 °C and 5% CO_2 for 24 h. TIL-enriched non adherent cells were collected, passed through a 70 μM nylon cell strainer (Miltenyi Biotec) and immediately cryopreserved in 10% DMSO (Sigma–Aldrich). Lung CAFs used for the *in vitro* experiments of hMENA(t) depletion were obtained from fresh NCSLC tumor specimens of patients undergoing curative surgery at the Regina Elena National Cancer Institute as previously reported[26] and cultured in Dulbecco's modified Eagle medium (DMEM Gibco, Invitrogen) supplemented with 1% (vol/vol) penicillin/streptomycin, 1% glutamine and 5% (vol/vol) inactivated fetal bovine serum (FBS) at 37 °C in 5% CO_2 95% air-humidified atmosphere. The isolated CAFs exhibited typical feature of spindle-like mesenchymal cells and Real Time Quantitative Polymerase Chain Reaction (qRT-PCR) analysis confirmed that these cells expressed CAF markers such as Fibroblast activation protein alpha (FAP), Actin alpha 2 smooth muscle (ACTA2), Platelet derived growth factor receptor beta (PDGFRB) and Podoplanin (PDPL), were negative for Epithelial cell adhesion molecule (EPCAM) and express various level of hMENA(t) (Supplementary Figure S1). Tumor tissues employed for Nanostring analysis were from 12 treatment naïve patients resected with curative intent at the Regina Elena National Cancer Institute and successively treated with ICB including nivolumab and pembrolizumab in the period from 2016 to 2019, approved by the ethics committee of the Regina Elena National Cancer Institute, and written informed consent was obtained from all patients. Depending on the date of surgical resection, molecular testing was performed by qRT-PCR (patients who received surgery before 2016) or Next Generation Sequencing (NGS) analysis adopting the diagnostic gene panel "Oncomine Solid Tumor DNA kit (CE-IVD) (Thermo Fisher Scientific), for patients who received surgery after 2016 or Oncomine Focus Assay (OFA, Thermo Fisher Scientific, Inc.) for patients after 2019.

qRT-PCR (Applied Biosystems 7500) with TaqMan probes (CE-IVD EntroGen kit) was limited to Epidermal Growth Factor Receptor (EGFR) and Kirsten Rat Sarcoma Virus (KRAS) genes. For EGFR Test the following mutations was evaluated: Exon 19 deletions; Exon 21 L858R; L861Q; Exon 18 G719A/S/C; Exon 20 T790M; S768I; Exon 20 insertions. For KRAS test the assay was limited to the following mutations: Exon 2: G12D, G12V, G12R, G12C, G12S, G12A, G13D. Exon 3: Q61R, Q61H, Q61L. Exon 4: K117X, A146X.

Oncomine Solid Tumor DNA kit is able to identify more than 1900 mutations (SNV, indels) in 22 genes. The OFA panel can identify hotspot mutations, including SNVs, indels (35 genes), CNVs (Copy Number Variations, 19 genes), and 23 fusion drivers that are commonly implicated in human cancers and relevant to targeted treatment of solid tumors.

Fluorescence in situ hybridization (FISH), to evaluate translocation of the Anaplastic Lymphoma Kinase (ALK) and ROS proto-oncogene 1 (ROS1) genes, was performed by using the ZytoLight® SPECDual Color Break Apart Probes and ZytoLight® FISH-Tissue Implementation Kit (ZYTOVISION) according to the manufacturer's instructions. The ALK and ROS1 probes included a mixture of a green fluorochrome labeled polynucleotides targeting sequences mapping in 2p23.1-p23.2 and 6q22.1, respectively and an orange fluorochrome labeled polynucleotides targeting sequences mapping to 2p23.2 in ALK and 6q22.1 in ROS1.The slides were analyzed by using a fluorescence microscope (×100). An average of 100 nuclei was considered within the invasive component of tumor tissue. A distance ≥2 signals diameter between green and orange separated signals were considered ALK and/or ROS1 translocated.

Ethics statement

The study and the informed consent obtained from enrolled patients was reviewed and approved by the local ethics committee (Protocol CE/594/11 on 11/03/2011 and 058.IFO_AOO.REGISTRO UFFICIALE.U.0012817.20-11-2017) and by the Comitato Etico Centrale IRCSS Lazio: Studio 'ACC LUNG2' (Prot. Number 1152/18).

Whole-Exome Sequencing Analysis

Fastq were mapped against the reference genome (GRCh38) using the nf-core/sarek pipeline.[30] Obtained bam files were processed with GATK toolset[31] following GATK best practices: Duplicated reads were marked with the "MarkDuplicates" command, quality score base recalibration was computed with the BaseRecalibrator command and applied with "applyBQSR" function. Variant calling was performed using Mutect2 with Gnomad population frequencies and a panel-of-normal for germline references. Identified variants were filtered using the following filters: Filter = "PASS", Variant Allele Frequency >0.05.

Immunohistochemical analysis

Several biological variables were evaluated by immuno-histochemistry. In particular, consecutive 4 μm sections were stained with pan-hMENA antibody (clone A351F7D9; Millipore, MAB2635) that recognizes all hMENA isoforms, including hMENAΔv6, and with a specific monoclonal hMENA[11a] antibody produced and validated by our group.[22] To visualize lymphocytes B and T, anti-CD20 (clone L26; Ventana, Roche Diagnostics) and anti-CD3 (clone 2GV6; Ventana, Roche Diagnostics) antibodies were utilized respectively. CXCL13 detection was obtained by the use of human CXCL13 Antibody (AF801 R&D Systems). CAF were visualized by the staining with alpha-SMA antibody (Clone ASM-1 NCL-L-SMA; Leica Biosystems) and FAP (ab207178; Abcam). Immunoreactions were revealed by UltraView DAB System Ventana Ultra platform (Ventana, Roche Diagnostics). Immunostained whole tissue slides were digitized, at a magnification of at least 20×, using a Leica Aperio AT2 scanner with Aperio eSlideManager and analyzed with Aperio ImageScope (Leica Microsystems). Slides were analyzed and scored independently by three different observers, blinded to the clinical data (FDM, EG and PV). Tumor area and tumor marginal zone were identified in hematoxylin and eosin (H&E) sections by a pulmonary pathologist. TLS were identified as aggregate of CD20 B cells surrounded by CD3 lymphocytes and were manually and/or digitally counted in the tumor area (TLS-IT) and peritumoral area (TLS-PT) of sections analyzed. The manual and digital counting were overlapping. For digital counting, the pathologist manually defined and annotated the selected regions of interest (ROIs), which included only the tumor region and, when feasible, the tumor marginal zone. The ROIs were subsequently analyzed using a laboratory developed and customized Aperio Nuclear v9 algorithm (Leica), specifically trained to identify the CD20 B-cell aggregate staining (TLS) (TLS V1.1_2) (representative image in Supplementary Figure S2). TLS presence was scored on a four-tiered scale: 0, no TLS; 1 = 1–10 TLS; 2 = 10–20 TLS; 3 > 20 TLS. Positive cases were considered with score 2–3 for TLS PT and 3 for TLS IT on the basis of the cut-off able to split patients into groups with different outcome probabilities. Stromal hMENA(t) expression was scored using a scale from 0 to 3 (score 0: no staining, score 1: weak, 2: moderate, and 3: strong). For statistical analysis grades 0–1 were merged and labeled as "Low", where grades 2–3 were combined and labeled as "High". hMENA[11a] and FN1 expression of the cases considered were already described.[24,32] For double immunostainings, sections were subjected to sequential rounds of single-marker immunostaining and the binding of the primary antibodies was revealed by the use of specific secondary antibodies conjugated with different enzymes. The following primary antibodies were adopted for IHC on human tissues: Activation-induced cytidine deaminase (AID, clone EPR23436-45;

Abcam), CD21 (clone 2G9, Leica Biosystems). Immunohistochemical staining was revealed using Novolink Polymer Detection Systems (Novocastra) and DAB (3,3'-Diaminobenzidine, Novocastra) as substrate chromogen. Double immunohistochemical staining was performed by applying SignalStain®Boost IHC Detection mouse alkaline phosphatase-conjugated and Vulcan Fast Red as substrate chromogen. We performed a semi quantitative approach to evaluate the density and the distribution of the TLS on the basis of the intra and peritumoral topographic localization and their different composition in terms of cellular elements based on the expression of AID and CD21. All Abs were titrated, and the appropriate saturating concentrations were used. PD-L1 immunoreactions were obtained by PD-L1 pharmDx monoclonal mouse antibody (clone 22C3, Agilent-Dako) and revealed by using the EnVision FLEX visualization system on Autostainer Link 48 (Agilent). PD-L1 protein expression in NSCLC was determined by using the Tumor Proportion Score (TPS). TPS* Tumor Proportion Score (number of PD-L1 positive tumor cells/total number of viable tumor cells) x100; TPS: <1%; TPS: 1–49%; TPS: ≥50%.

Multiplex IHC
Multiplex IHC was performed in selected samples decorated with the Opal™ 4-Color Manual IHC kit (Akoya Bioscence) according to the manufacturer instructions. Tissues were prepared using the standard fixation and embedding technique until the creation of 4 μm section placed on a TOMO™ slide. With this staining we have highlighted: B lymphocytes with anti-CD20 antibody (clone L26, Leica Biosystems) visible with Opal 520 Fluorophore; tumor cells with pan-hMENA antibody (clone A351F7D9; Millipore, MAB2635) visible with Opal 690 Fluorophore; stromal area with α-SMA antibody (ab5694; Abcam) visible with Opal 570 Fluorophore; nuclei were counterstained with 4',6-diamidino-2-phenylindole (DAPI) (Spectral DAPI solution, Akoya Biosciences). Images were obtained using Zeiss LSM 880 with Airy scan confocal laser scanning microscope equipped with a 20× air objective.

Analysis of patients with lung cancer from TCGA
The UCSC Toil RNA-Seq Recompute data[33] from the analysis of The Cancer Genome Atlas (TCGA) lung (LUSC and LUAD) program were used for the gene and isoform expression levels and downloaded using the Xena browser (cohort: TCGA Pan-Cancer (PANCAN)).

TCGASpliceSeq[34] was used to download the LUNG RNASeq data for transcript splicing variation. For each Lung Squamous-Cell Carcinoma (LUSC) (n = 561) and Lung Adenocarcinoma (LUAD) (n = 583) patient, the splice events for ENAH gene with specific percent spliced-in (PSI) values were downloaded from the TCGASpliceSeq website interface. PSI is the ratio of normalized read counts indicating inclusion of a transcript element over the total normalized reads for that event (both inclusion and exclusion reads). A total of 5 splice events were identified for ENAH (1 alternate acceptors site and 4 exon skips) and two of these events, representing the skip of exon 6 and 11a, were used to characterize the hMENAΔv6 isoform.

Overall Survival (OS) data and clinical information were derived from the TCGA Pan-Cancer Atlas publication by Liu and colleagues[35] and downloaded from the Genomic Data Common repository (https://gdc.cancer.gov/node/905/). For the analysis of OS, patients at stages 1 and 2 of the disease, as well as stages 3 and 4 based on the American Joint Committee on Cancer (AJCC), were considered. The analysis included patients for whom survival data were available and who had a minimum follow-up of 1 month. The patients were stratified into two groups, hMENAΔv6^{high}/FN1^{high} and hMENA11a^{high}/hMENAΔv6^{low}, on the basis of the PSI values for exon 6 and 11a and the expression levels for FN1 gene and 11a isoform. The receiver operating characteristic (ROC) was applied to the continuous variable to estimate the most appropriate cut-off values able to split patients into groups with different outcome probabilities. In detail, patients with a PSI value less than the cut-off value in the cohort for both exon 6 and 11a were classified as hMENAΔv6^{high} (indicating the patients with a minor percentage of inclusion of the exons in the transcripts of the sample); patients with isoform hMENA^{11a} mRNA expression levels higher than the cut-off value in the cohort were classified as hMENA11a^{high}; patients with FN1 mRNA expression levels higher than the cut-off value in the cohort were classified as FN1^{high}. Thus, patients with both hMENAΔv6^{high} and FN1^{high} were classified as hMENAΔv6^{high}/FN1^{high}; patients with both hMENAΔv6^{low} and hMENA11a^{high} were classified as hMENAΔv6^{low}/hMENA11a^{high}. The final cohort consists of 440 patients with LUNG cancer. Survival curves were estimated using the Kaplan–Meier method, and statistical differences were tested using the logrank test; P values < 0.05 were considered to be statistically significant.

Somatic mutations for patients with LUNG cancer were downloaded from Xena browser (https://xenabrowser.net/). Missense and nonsense mutations, along with frame shift deletions and insertions within the oncogenes sourced from the TCGA LUAD and LUSC cohorts, were considered. Fisher's exact test was utilized to evaluate the potential enrichment of gene mutations within hMENA11a^{high}/hMENAΔv6^{low} and hMENAΔv6^{high}/FN1^{high} patient classes.

Furthermore, the cohort was stratified in CAF^{high} and CAF^{low} on the basis of the ECM-myCAF gene signature reported[14] and in TLS^{low} and TLS^{high} on the basis of two different signatures: a classic cytokine-based signature[36] and a recent reported Ig-enriched signature from Meylan et al.[12] The geometric mean of

the expression of genes belonging to each signature was used as the score for the respective gene signature. The median of each signature score was used to stratify the patients in 2 groups. In detail, patients with CAF score above the median value and TLS score below the median value were classified as CAF^{high}/TLS^{low}; patients with CAF score below the median and TLS score above the median were considered as CAF^{low}/TLS^{high}. The stratification process was performed using both the cytokine-base and Ig-enriched TLS signatures independently, coupled with the ECM-myCAF signature. Fisher's exact test was used to assess whether the hMENA11a^{high}/hMENAΔv6^{low} class of patients was highly enriched in CAF^{low}/TLS^{high} patients.

All analyses were performed using R statistical environment (v4.1.3).

Cell lines and cultures

The human lung cancer cell lines A549 (CCL-185, RRID: CVCL_0023), H1299 (CRL-5803, RRID: CVCL_0060), H1650 (CRL-5883, RRID:CVCL_1483), H460 (NCI-H460 (HTB-177, RRID:CVCL_0459), CALU-1(HTB-54, RRID:CVCL_0608) and T2 (CRL-1992, RRID:CVCL_2211) cell line were purchased from American Type Culture Collection (ATCC). The human lung H358 and H1437 cancer cell lines were kindly provided by Dr. R.P. Carstens (Department of Medicine, University of Pennsylvania School of Medicine, Philadelphia, PA 19104). Normal lung fibroblasts, IMR-90 (RRID:CVCL_0347) were obtained from ATCC.

The cell lines were authenticated by chromosomal analysis (BMR Genomics). All cell lines were routinely checked for mycoplasma using Mycoplasma PCR Reagent set (Euroclone). The cells were maintained in RPMI 1640 Medium (Euroclone), supplemented with 10% FBS (Euroclone), 1% Glutamine, 1% Penicillin/Streptomycin (Euroclone), and incubated at 37 °C in a 5% CO_2 air-humidified atmosphere.

Purified human recombinant LIGHT (R&D, Minneapolis) was used at 50 ng/mL in serum-free medium for 24 h.

Harvesting tumor-conditioned media

Conditioned media (CM) were obtained from tumor cell line H1650 transfected with hMENA^{11a} specific siRNAs or with non-targeting control siRNAs. Cell culture supernatants were collected after 24 h, filtered, aliquoted and immediately stored at −80 °C. TILs were thawed and left in RPMI plus 10% Human Serum (HS) at 37 °C a 5% CO_2 for 24 h before use. The day after, viability of cells was determined by the use of trypan blue. After washing, lymphocytes were placed in 48-well plate, at 2×10^5 cells/well, and cultured with undiluted tumor-derived CM for 24 h. Golgistop (BD Bioscience, 554,724) and Golgiplug (BD Bioscience 555,029) were added the last 5 h before flow cytometry staining.

Cytokine analysis

Levels of 40 different chemokines and cytokines were evaluated by Pro Human Cytokine 40-Plex Assays panel (Bio-Rad, Hercules, CA, USA), according to the manufacturer's instructions. Cytokines were quantified on the Luminex platform using the Bio-Plex MagPix instrument (BioRad, Hercules, CA, USA) and the Bio-Plex Manager MP software was used for data acquisition and analysis. All the samples were run in duplicate and ten-point standard curve, positive, negative sample were run for each cytokine. Determinations that were designated "Out of Range Below" (i.e., below the limit of quantification) by the analytical software were arbitrarily filled with a zero value.

Flow cytometry

Cell staining was performed using various combinations of the following Abs: CD3-BV650 (BD, clone UCHT1), CD4-BV786 (BD, clone SK3), CD8-APC-H7 (BD, clone SK1), CD103-BV605 (BD, clone Ber-ACT8), CD69-BV421 (BD, clone FN50), CD19-APC-H7 (BD, clone HIB19), CD24-PE (BD, clone ML5), CD27-PE-Cy7 (BD, clone M-T271), CD38-PerCP-Cy5.5 (BD, clone HIT2), IgD-FITC (BD, clone IA6-2), CXCL13-APC (Invitrogen, clone 53,610). Surface staining was performed for 30 min at 4 °C. Intracellular staining was performed by the use of Intrasure kit (BD) according with the manufacturer instructions. Cells were immediately acquired in the BD FACSCelesta flow cytometer and analyzed by the use of BD FACSDiva software (RRID:SCR_001456).

Small interfering RNA (siRNA)

3×10^5 cells/well in exponential growth phase were plated in 6-well plates. The next day, cells were transfected with 20 nmol/L of hMENA(t)-specific pooled siRNA duplexes (siGENOME SMARTpool Human ENAH), or 20 nmol/L of mix of three siRNAs each matching 21 nucleotides within the 11a exon sequences[37] or 20nmol/L of ON-TARGETplus Nontargeting Control Pool (GE Healthcare, Dharmacon) using Lipofectamine® RNAiMAX Transfection Reagent (Invitrogen) according to the manufacturer's protocol. The specific effect of hMENA(t) silencing was validated using transient transfection of MISSION® shRNA Plasmid DNA–ENAH human–TRCN0000303614 (Sigma–Aldrich). The effects of silencing were evaluated at 72 h from the transfection.

Transfections

3×10^5 cells/well were plated in six-well plates and the next day transfected with 2.5 µg/mL of pcDNA3-hMENA^{11a}, pcDNA3-hMENAΔv6, or with empty vector (pcDNA3), using LipofectAMINE 2000 (Invitrogen).

RNA extraction and real-time PCR

Total RNA was isolated from cells using TRIzol reagent (Invitrogen). Reverse transcription was carried out using

first-strand cDNA synthesis kit (GE Healthcare). Quantitative RT-PCR (qRT-PCR) reactions were performed in triplicates using TaqMan Universal PCR Master Mix No AmpErase UNG (Applied Biosystems, 4324018) in ABI Prism 7500 Real-time PCR instrument (Applied Biosystems). TaqMan Gene Expression Assays (Applied Biosystems) were used for amplification and quantification of ENAH (Hs00403109_m1), LTβR (Hs01101194_m1), FAP (Hs00990791_m1), ACTA2 (Hs05005341_m1), PDGFRB (Hs01019589_m1), PDPL (Hs00366766_m1), EPCAM (Hs00901885_m1), Integrin beta 1 (ITGB1) (Hs00559595_m1) and Hypoxanthine Posphoribosyltransferase1 (HPRT1) (Hs99999909_m1), used as an endogenous control. hMENA[11a] mRNA quantification was performed with custom designed probe and primers from Applied Biosystems (TaqMan MGB Probe: 5′-CTCCAGACGGGATTCT-3'; forward primer: 5′-ATGGCAGCAAGTCACCTGTTAT-3'; reverse primer: 5′-TGTAATGAATCATAGGACCTGTTGTCAAAA-3′). The comparative Ct method (2−∆∆/Ct method) was used to determine changes in relative levels of different genes.

RNA-seq
Total RNA was extracted from cell lines using Qiazol (Qiagen), purified from DNA contamination through a DNase I (Qiagen) digestion step and further enriched by Qiagen RNeasy columns for gene expression profiling (Qiagen). Quantity and integrity of the extracted RNA were assessed by NanoDrop Spectrophotometer (NanoDrop Technologies) and by Agilent 2100 Bioanalyzer (Agilent Technologies), respectively. RNA libraries for sequencing were generated in triplicate using 500 ng of RNA for each sample according to the Illumina TruSeq Stranded Total RNA kit with an initial ribosomal depletion step using Ribo Zero Gold (Illumina). The libraries were quantified by qRT-PCR and sequenced in paired-end mode (2 × 75 bp) with NextSeq 500 (Illumina). For each sample generated by the Illumina platform, a pre-process step for quality control was performed to assess sequence data quality and to discard low-quality reads.

RNA-seq data analysis
Processing of raw data from RNA-Seq experiments was performed on RNA-Seq Analysis Pipeline (RAP) web tool[38] using default parameters and HG19 as reference genome. Differentially expressed genes with adjusted P value <0.05 (Bonferroni correction) were considered significantly modulated between each condition. Plots were generated using the R statistical environment (v4.0).

Fibronectin assembly assay
The rate of fibrillogenesis was analyzed by Fibronectin Assembly Assay in cell lines and in CAFs. Briefly, cells were plated into 8-well chamber μ-slides in the presence of 10 μM of cycloheximide (Sigma) 37 °C 5%, CO₂. After

6 h, the medium was changed and FN-488 HiLyte 488 labeled (Cytoskeleton) was added to achieve a final concentration of 4 μg/mL for 18 h. The cells were washed twice with PBS, fixed and then incubated with DAPI (Bio-Rad) for nuclei staining. Images were obtained using Spettral confocal microscope Zeiss LSM 880C, Airyscan. Lasers 405, 488, nm were used to excite the fluorophores. The Zeiss Zen control software (Zeiss) was used for image analysis.

Western Blot analysis and antibodies
Protein extraction and Western Blot (WB) analysis were carried out as previously described.[22] The following primary antibodies were used: rabbit hMENAΔv6,[22] rabbit Pan-hMENA,[39] mouse hMENA[11a],[22] Nuclear factor kappa-light-chain-enhancer of activated B cells (NF-kB2) p100/p52 (Cell Signaling, 4882), pNF-kB p65 (clone 93H1, Cell Signaling), NF-kB p65 (clone D14E12, Cell Signaling), mouse Heat Shock Protein 70 kilo Daltons (HSP-70) (clone W27, Santa Cruz), mouse Actin (clone AC-40, Sigma–Aldrich), mouse Fibronectin 1 (clone IST-4, Sigma–Aldrich), rabbit Tubulin (clone 11H10, Cell Signalling). Densitometric quantitation of antibodies immunoreactivity used in WB analysis was determined by Image J 1.49v program (RRID:SCR_003070) and normalized in comparison with the β-actin, α-Tubulin or HSP70 immunoreactivity.

ELISA assay
Levels of CXCL13 in conditioned media were determined by Enzyme-linked immunosorbent assay (ELISA) (EA 100469, Origene) after 48 h from silencing or transfection of CAFs and IMR-90 as described above. The culture medium was collected and CXCL13 level was detected according to the manufacturer's protocol. Values were corrected for the cell protein amounts.

NanoString analysis
Gene-expression profiling was performed using a custom 770 gene NanoString PanCancer IO 360 Panel comprising immune-related genes and genes pertaining to common cancer signaling pathways and including probes for the three hMENA isoforms, LTβR and FN1. The RNA was extracted from 5 μm Formalin-Fixed, Paraffin-Embedded (FFPE) tissue sections using All-Prep DNA/RNA FFPE kit (Qiagen). The quantity and purity of the RNA was assessed with the NanoDrop spectrophotometer. In case of low 260/230 ratios the samples were re-purified by chloroform and subsequent ethanol precipitation. The quality of the RNA was controlled with the Bioanalyzer employing the Agilent RNA 6000 Pico or Nano Kit (Agilent Technologies). As input we used 100 ng total RNA following the manufacturer's instructions. After the Codeset hybridization the samples were washed and loaded on the cartridge within the Prep Station and subsequently analyzed with the nCounter Digital Analyzer.

Normalized expressions of transcripts were split into high/low expression using the ROC approach, to estimate the most appropriate cut-off values able to split patients into groups with different outcome probabilities. Relative expression results were plotted against clinical response, defined as poor response (PR) versus good response (GR). "Selected" samples were those that were high hMENAΔv6, low hMENA[11a], high FN1 and low LTβR. "Other" samples were those did not satisfy the "Selected" conditions. P values were determined by performing the Fisher's Exact test on a contingency table with columns indicating clinical benefit and rows indicating Selected/Other status.

PD-L1 score was evaluated by grouping the normalized counts from the Nanostring profiling into 3 expression level groups based on the ranking of CD274 expression levels.

Skin cutaneous melanoma (SCKM) validation cohort

Data for the SCKM validation cohort were from Liu and coauthors.[40] The analysis was completed from fastq to plots using a single Reproducible Analyses Framework and Tools (RAFT)-built Nextflow DSL2 pipeline. Briefly, RNA sequencing FASTQ data files of pretreated samples from 12 ICB treated patients, were adapter-trimmed using Trim-Galore v0.6.2 https://www.bioinformatics.babraham.ac.uk/projects/trim_galore/ (Trim Galore, RRID:SCR_011847), aligned to GRCh38/v103 using STAR v2.7.0 (STAR, RRID:SCR_004463) and counted using Salmon v1.1.0.[41] ENST counts were converted to HGNC gene symbols base on the Vincent Lab conversion table (https://sc.unc.edu/benjamin-vincent-lab/gene-sigs/human_ensembl_to_hgnc_entrez). Prior to analysis, all transcript counts were upper quartile normalized and log2 transformed. ENST counts for two transcripts of interest and HGNC counts for two genes of interest were split into high/low expression using the ROC approach, as for the discovery cohort. Relative expression results were plotted against Clinical Benefit, defined as complete/partial response and stable disease versus progressive disease. "Selected" samples were those that were high hMENAΔv6, high FN1 and low LTβR. "Other" samples were those did not satisfy the "Selected" conditions. P values were determined by performing the Fisher's Exact test on a contingency table with columns indicating clinical benefit and rows indicating Selected/Other status.

Triple-negative breast cancer single-cell RNAseq analysis

Raw read scRNAseq data of 12 TNBC pre-treatment samples were mapped to the human genome GRCh38 using cell ranger v3.1.0.[42] The number of junction reads with a unique UMI in fibroblasts in support of exclusion or inclusion of exon 6 hMENA were counted. PSI values for exon 6 hMENA were calculated in each sample, while LTβR expression was calculated based on the number of mapped reads in fibroblasts per sample while normalizing to count per million (CPM) reads. PSI values for exon 6 hMENA and CPM values for LTβR gene were split into high/low expression using the ROC approach, as for the discovery cohort. Relative expression results were plotted against anti-PD-1 responders (i.e., T cell expanded, 'E') versus non-responders (i.e., T cell non-expanded, 'NE'). "Selected" samples were defined as high hMENAΔv6 and low LTβR expression. "Other" samples are those did not satisfy the "Selected" conditions. P values were determined by performing the Fisher's Exact test on a contingency table with columns indicating anti-PD-1 non-responders and rows indicating Selected/Other status.

Spatial transcriptomics

We applied GeoMx DSP on two cases of ICB-treated patients of our experimental cohort, one GR (with TLS IT localization) and one PR (with TLS PT localization). Five μm FFPE tissue sections were processed according to the GeoMx DSP protocols and incubated overnight at 37 °C with the probes of the GeoMx® Cancer Transcriptome Atlas (CTA) panel with the addition of customer probes targeting three different hMENA splice variants (hMENA[11a]: ACGGGATTCTCCAAGGAAAAATCAGATTGTTTTTGACAACAGGTCCTATG; hMENA: AGACCAAAATCCACACCCTTATCACAGCCCAGTGCCAATGGAGTCCAGAC; hMENAΔv6: TGGCATTGTCTTGGGACCACTTGCACCTCCACCTCCTCCACCACTCCCAC). The slides were then stained with fluorescent labeled CD45 and Pan-cytokeratin (Pan-CK) antibodies (GeoMx solid tumor TME morphology kit human RNA compatible) together with SYTO 13 (nuclear stainer). Subsequently, the slides were loaded into the GeoMx DSP instrument. Regions of interest (ROIs) were selected as representative parts of the tumor across the whole slide in regions close to TLS area, as morphologically defined by a pathologist. The ROIs were further segmented based on the Pan-CK staining to differentiate tumor cells versus stroma areas. After ultraviolet illumination, UV-cleaved oligos from the ROIs were collected into 96-well plates and dried for 1 h at 65 °C. The collected aspirates were rehydrated and a part transferred to a plate to perform via PCR the library preparation with Seq Code primers. Libraries were purified and combined in pools according to their ROI size. Library pools were quality controlled on a TapeStation 4200 and quantified by qPCR before sequencing on the Illumina NovaSeq 6000 instrument. FASTQ sequencing files were processed into digital count conversion (DCC) files using BaseSpace™ Sequence Hub and then uploaded onto the GeoMx DSP.

After ROIs/probes quality check (QC) according to NanoString's recommendations and principal component analysis to eliminate potential outliers, Areas of Illumination (AOI) raw counts were normalized using

Q3 normalization method. The differential gene expression analysis was performed with the *"limma"* (v3.50.3) R package, adjusting P values for multiple testing using the Benjamini-Hochberg correction. Volcano plot showing differentially expressed genes was generated using *"ggplot2"* (v3.4.1) R software package. All computational analyses were performed in the R statistical environment (v4.1.2).

Statistical analysis

Descriptive statistics were used to summarize pertinent study information. Normality distribution of data was assessed by Wilk–Shapiro tests and where necessary by Quantile–quantile plot (QQ-plots). The normality of the data distributions and homogeneity of variances were evaluated for appropriateness prior to conducting the statistical tests. Depending on the distribution of the data, parametric or non-parametric tests were used as indicated in Figure legends. The associations between categorical biological variables were tested by Fisher's exact test (see Fig. 1d and e and Fig. 4a–g). In case of quantitative variables, the comparison between matched P, N and T sites were evaluated with non-parametric Friedman test (see Fig. 3 and relative legend). For the comparison of the two independent groups (IT-versus IT + patients), non-parametric exact Mann–Whitney U-tests was used (see Fig. 3 and relative legend). The correlation between quantitative variables was tested by non-parametric Spearman test. The correlation coefficients were interpreted in a qualitative manner according to the following classification criteria: a) Strong correlation (high degree): if the coefficient value lies between $\pm$ 0.50 and $\pm$1). Medium correlation (moderate degree): if the value lies between $\pm$ 0.30 and $\pm$0.49 c) Small correlation (low degree): when the value lies below $\pm$ 0.29. d) No relationship: Correlation Coefficient = 0.

For *in vitro* experiments, the statistical significance was calculated using two-tailed Student's t-test for two-sample comparisons or by one-way ANOVA followed by Tukey's procedures for multiple comparisons, as generally applied for this type of data.[43,44] Statistical significance was defined as $P < 0.05$ (see Fig. 5 and Supplementary Figure S8).

The ROC was applied to the continuous variable in order to estimate the most appropriate cut-off values able to split patients into groups with different outcome probabilities. For the 94 early patients with NSCLC, Disease-Free Survival (DFS) and OS were calculated by Kaplan–Meier product-limit method from the date of the surgery until death. If a patient was alive, DFS and OS were censored at the time of the last visit. The log-rank test was used to assess differences between subgroups. Statistical significance was defined as $P < 0.05$. Univariate analysis was carried out and the Odds Ratio (OR), Hazard ratio (HR) and the 95% Confidence interval (95% CI) were estimated for Sex; Age; Grading;

pT stage; Histotype; hMENA(t); hMENA[11a]; TLS IT; TLS PT; Stromal FN1; Hyb-hMENA[11a]; Presence of CD3+ lymphocytes into the tumor nests using the univariate logistic and Cox regression models, respectively. To identify the key factors that affect the outcomes and explore the relationships between multiple variables, a multivariate logistic regression and multivariate Cox regression model were developed using stepwise regression (forward selection, enter limit and remove limit, P = 0.10 and P = 0.15, respectively), considering the variables significant at univariate analysis (statistical significance was defined as P < 0.05). For any factor–outcome association, none of the other variables in the model can be considered potential mediators, therefore we are not concerned about over-adjustment. Additionally, we took into account the interactions among significant investigational variables during the development of the multivariate model. The proportional hazards (PH) assumption was checked using statistical tests and graphical diagnostics based on the scaled Schoenfeld residuals. For the Cox model the time from the date of the surgery until death was considered for each patient. If a patient had not experienced an event (death), the data were censored at the time of the last visit.

The SPSS (21.0) (SPSS, RRID:SCR_002865), MedCalc (12.7.5), GraphPad Prism 9 software (GraphPad Prism, RRID:SCR_002798) statistical programs were used for all analyses.
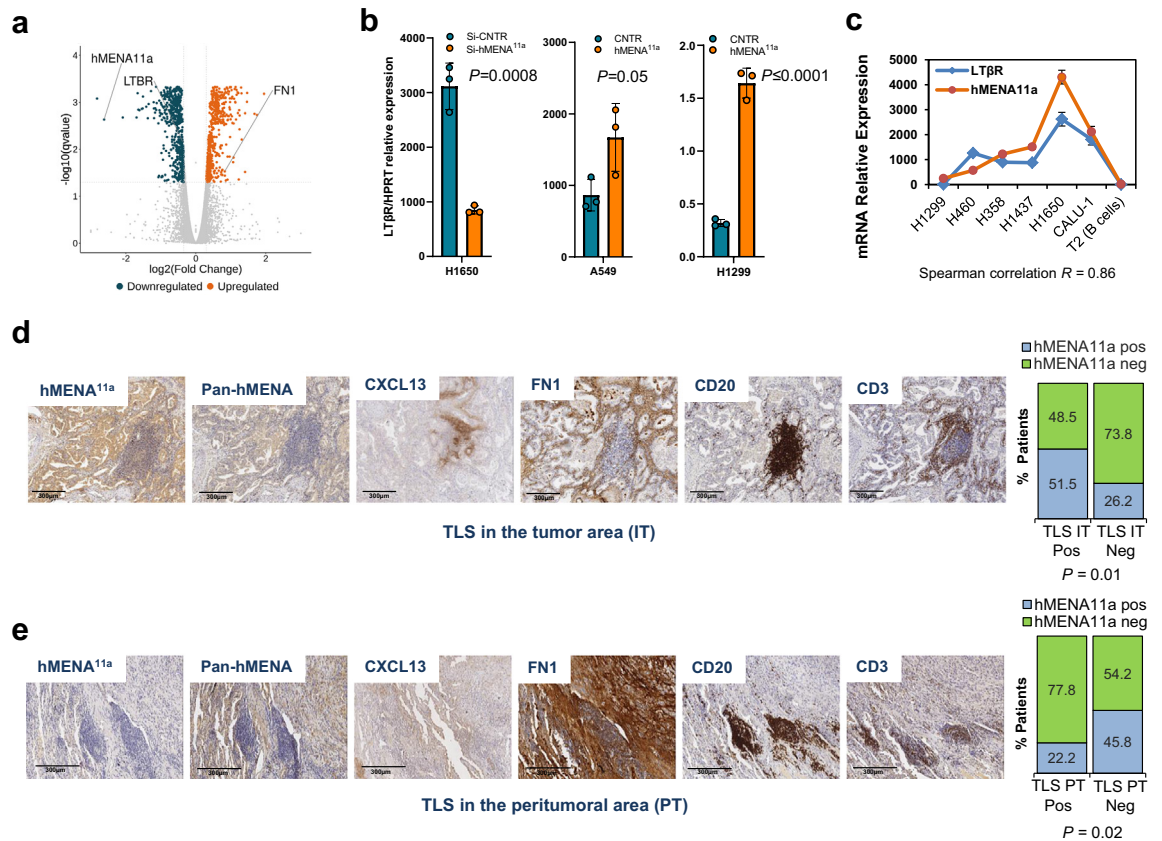
Role of the funding source

Results

The depletion of hMENA[11a] down-regulates LTβR and up-regulates FN1 in NSCLC cells. hMENA[11a] expression associates with intratumoral TLS and predicts survival of node-negative patients with NSCLC

Our previous data indicate that the expression of the epithelial-associated hMENA[11a] in tumor cells correlates with a low stromal level of FN1 in early node-negative NSCLC tissues and that these two parameters are associated with a longer survival of these patients.[24] To explore the mechanisms underlying the high hMENA[11a] expression and patient survival, we carried out RNA-Seq experiments in NSCLC cells silenced for hMENA[11a] with a pool of specific siRNAs previously characterized.[37] RNA-Seq of sihMENA[11a] H1650 NSCLC cells revealed that hMENA[11a] knock-down modulated several genes including the upregulation of FN1, and the downregulation of LTβR, a crucial molecule in the organization and maintenance of lymphoid tissues and able to support TLS development[45] (Fig. 1a).

Fig. 1: The depletion of hMENA[11a] down-regulates LTβR and up-regulates FN1. In node-negative patients with NSCLC, hMENA[11a] expression associates with intratumoral TLS. **a.** Volcano plots showing differentially expressed genes (q-value <0.05, n = 1096, GSE217451) in Si-hMENA[11a] versus control H1650 NSCLC cells (n = 3). Reported are the negative log10-transformed adjusted P values plotted against the log2 fold changes. Dots represent individual genes. **b.** qRT-PCR analysis of LTβR mRNA expression in the indicated cell lines transfected with control (Si-CNTR), and hMENA[11a] pool SiRNAs (Si-hMENA[11a]) or with plasmid control (CNTR) and hMENA[11a] expressing vector (hMENA[11a]). The control of hMENA[11a] expression in the transfected cells by WB is reported in Supplementary Figure S3a. Data are reported as the mean ± SD of technical triplicates which are representative of two independent experiments. P value was calculated by 2-tailed Student's t test. **c.** qRT-PCR analysis showed that LTβR and hMENA[11a] mRNA expression level correlate in NSCLC cell lines. The value of Spearman correlation is reported. **d.** Consecutive sections of a representative NSCLC primary tumor hMENA[11a] positive, showing low stromal FN1, TLS IT localization and high CXCL13. Magnification 8×. Scale bar 300 μm. Right, histograms relative to the IHC analysis of 94 node-negative NSCLC tissues showing that hMENA[11a] positive cases more frequently show TLS within the tumor area (TLS IT). **e.** Consecutive sections of a representative case of lung adenocarcinoma hMENA[11a] negative, showed high stromal FN1, TLS PT and low CXCL13. Right, histograms are relative to the IHC analysis of 94 node-negative NSCLC tissues showing that hMENA[11a] negative (hMENA[11a low]/hMENA (t)[high]) cases more frequently show peritumoral TLS (TLS PT). P value was estimated with Fisher Exact test.

After RNA-Seq data validation by qRT-PCR (Fig. 1b), we performed qRT-PCR in a panel of lung cancer cell lines and a strong correlation (Spearman correlation R = 0.86) between LTβR and hMENA[11a] emerged (Fig. 1c and Supplementary Figure S3b for the hMENA isoform protein expression). Conversely, when the hMENA[11a] negative A549 and H1299 cell lines were transfected with hMENA[11a] a significant increase of LTβR mRNA level occurs (Fig. 1b and Supplementary Figure S3a).

In view of these findings, and considering the specific prognostic relevance of hMENA[11a] observed in N0 patients, but not in advanced node-positive NSCLC cases, as assessed in both our internal cohort (Supplementary Figure S4) and LUAD and LUSC TCGA datasets (see below), we proceeded to analyze the presence and localization of TLS in the primary tumors of a cohort comprising 94 treatment-naïve N0 patients with NSCLC. The clinicopathological characteristics and relapse pattern of these patients are detailed in Supplementary Table S1 and Supplementary Figure S5, respectively. We firstly noted that CD20+ B cells were rarely scattered as occurs for CD3+ T cells, but rather found in aggregates surrounded by CD3+ T
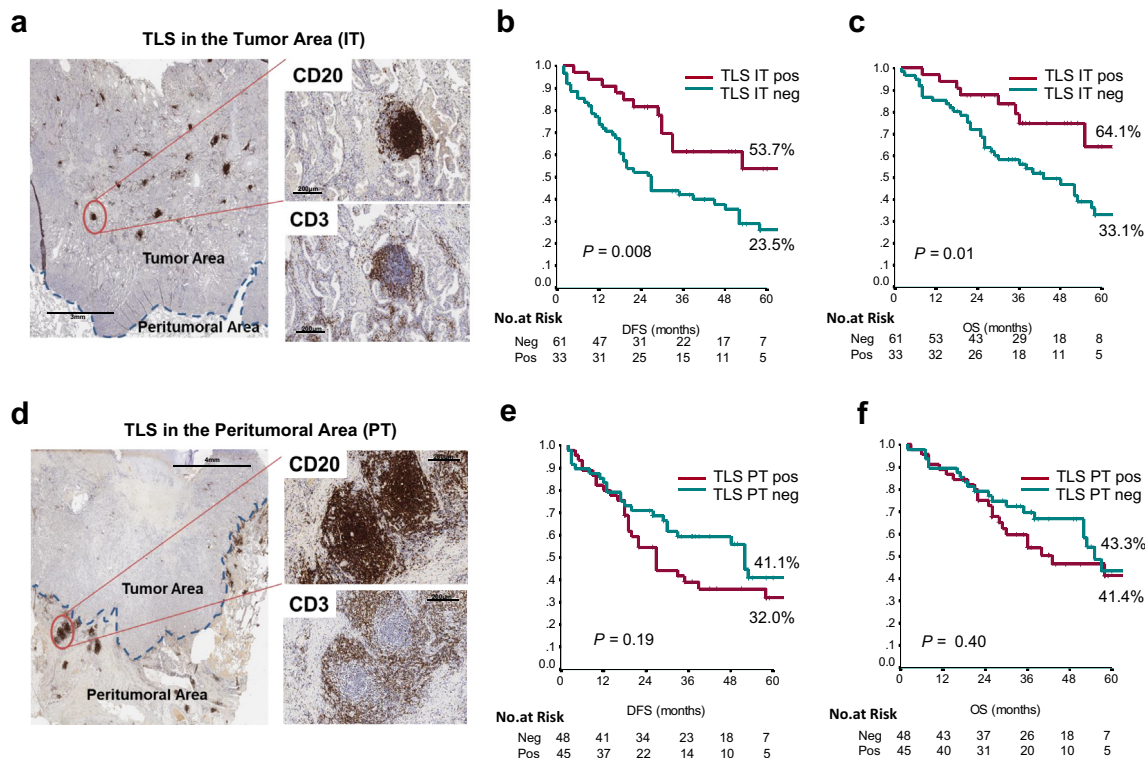
Fig. 2: **TLS organized within the tumor core are predictive of survival in 94 early patients with NSCLC. a.** Representative case of a lung ADC stained for B (CD20) and T (CD3) cells showing the presence of TLS within the tumor area (IT). **b and c.** Kaplan–Meier estimate of disease-free survival (DFS) (b) and overall survival (OS) (c) of resected, node-negative patients with NSCLC according to the presence of TLS IT. **d.** Representative case of an undifferentiated cancer of the lung stained as in A, showing the presence of TLS in the peritumoral region (PT). **e and f.** Kaplan–Meier estimate of DFS (e) or OS (f) of resected, node-negative patients with NSCLC according to the presence of TLS PT. P value was estimated with log-rank test.

lymphocytes. We then characterized these TLS for their maturation stage with CD21 to stain follicular dendritic cells and AID, the enzyme driving the immunoglobulin somatic hypermutation and class switch recombination, for the visualization of germinal center (GC) B cells. TLS presence was revealed in 65 cases of the 94 evaluated and were found to be highly heterogeneous for the expression of CD21 and AID. Indeed, poorly-organized cellular aggregates CD21−/AID− were detected along with primary follicle-like TLS with a network of follicular dendritic cells (CD21+/AID-) and mature TLS with a germinal center composed of CD21+ and AID+ cells (representative cases are shown in Supplementary Figure S6). We then analyzed TLS localization and found that 20 cases (22%) showed TLS only within the tumor area (intratumoral TLS, IT), 14 cases (15%) in both tumor (IT) and peritumoral area (PT), whereas in 31 cases (34%) TLS were excluded by the tumor area, but present in the PT region (Supplementary Table S1 and representative examples Fig. 2a and d). It has to be noted that TLS PT negative cases encompasses both TLS IT positive (20 cases) and TLS IT negative cases

(27 cases). TLS were detected in both ADC and squamous cell (SCC) tumors (57% versus 34%), and their exclusive IT localization occurred more frequently in adenocarcinomas (80% ADC versus 20% SCC), whereas PT localization was prevalently found in squamous cancers (36% ADC versus 48% SCC) (Supplementary Table S1).

hMENA[11a] negative versus hMENA[11a] positive tumors, as defined by the use of two antibodies, pan-hMENA and the specific hMENA[11a] and referred as Hyb-hMENA[11a,32] was associated with survival (Cox regression model HR = 6.006; P < 0.0001 for OS, Supplementary Table S2; HR = 3.908; Cox regression model P < 0.0001 for DFS, Supplementary Table S3). Of note, we found that hMENA[11a] positive cases more frequently showed TLS within the tumor area (TLS IT, Fig. 1d), and high expression of CXCL13 whereas hMENA[11a] negative cases showed peritumoral TLS (Fig. 1e). At univariate analysis, we evidenced that, among the variables evaluated and beyond hMENA[11a], the absence of TLS IT and the age of the patients >68 years, emerged as associated with survival (Supplementary Tables S2
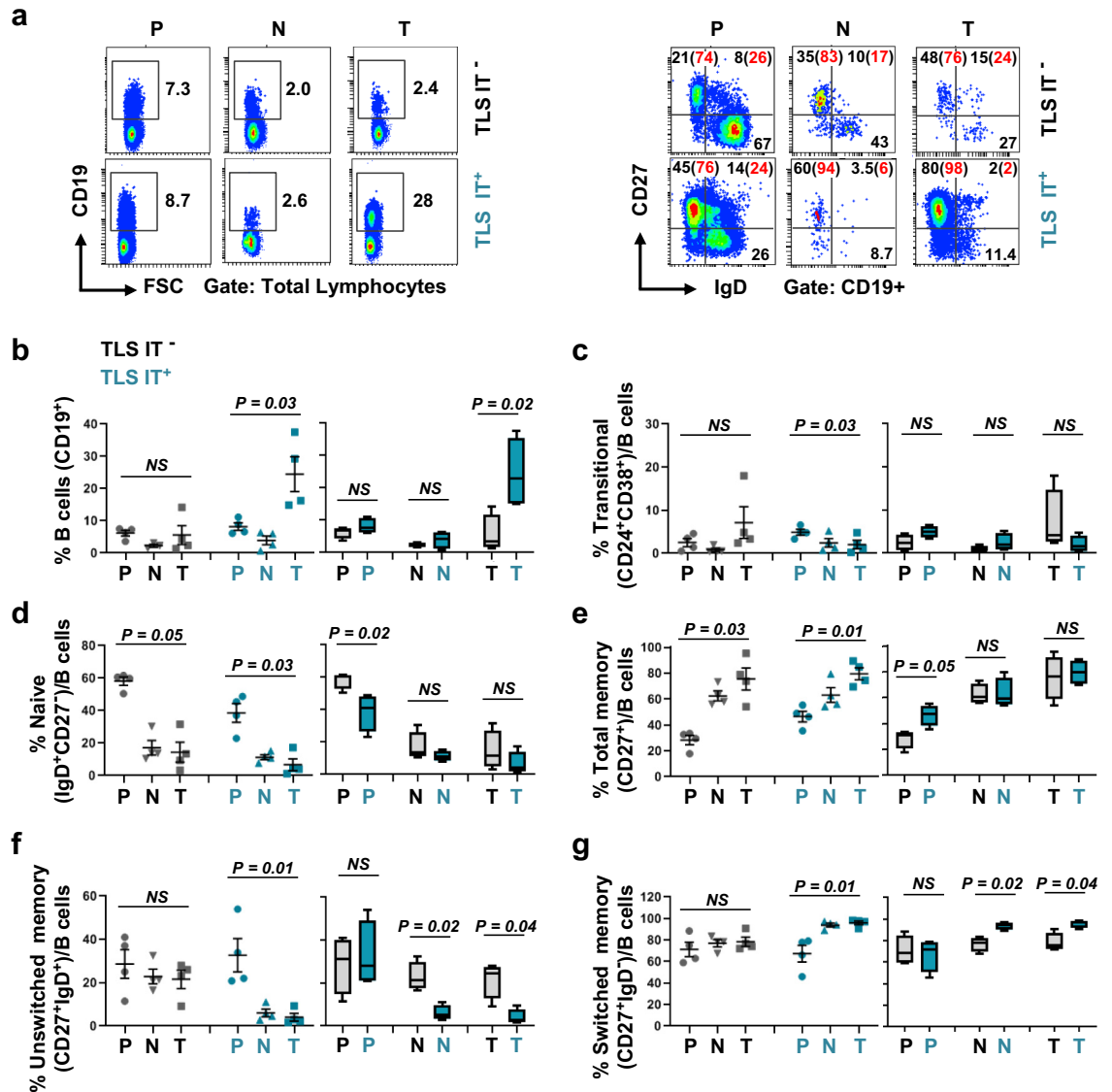
Fig. 3: **TLS located within tumor core (IT⁺) are associated with high percentage of switched memory phenotype B cells. a.** Representative dot plots showing CD19⁺ (left panel) and CD27 versus IgD staining (right panel), in *ex vivo* lymphocytes derived from PBMC (P), non-tumoral (N) and tumor tissues (T), of two patients with NSCLC non-possessing (IT-) or possessing (IT+) TLS within the tumor core. Percentages of different subsets are indicated as black numbers. Red numbers represent the proportion of switched (CD27⁺IgD⁻) or unswitched (CD27⁺IgD⁺) subsets within total memory B cells (CD27⁺). **b–g.** Pooled results from patients with TLS IT⁻ (grey color, n = 4) and TLS IT⁺ (blue color, n = 4) NSCLC showing the percentage of total B cells (CD19⁺) within the lymphocyte gate, and the principal B-cell differentiation subsets within CD19⁺ B cells. Transitional B cells (CD24⁺CD38⁺); Naïve (CD27⁻IgD⁺); Memory B cells (total CD27⁺); Unswitched memory B cells (CD27⁺IgD⁺); Switched memory B cells (CD27⁺IgD⁻). Left panels, comparison between matched P, N and T sites (non-parametric Fridman test), within IT⁻ or IT⁺ group; right panels, comparison between IT⁻ versus IT⁺ within the same site (non-parametric Mann–Whitney test). NS, not significant.

and S3). At multivariate analysis, the three variables remained significant independent predictors of outcome. No significant association was found between TLS IT and pathological variables, including the tumor grade (Supplementary Figure S7b), whereas TLS PT strongly associated with less differentiated tumors (i.e., higher tumor grade, Fisher exact test P < 0.0001) (Supplementary Figure S7c). Kaplan–Meier curves indicate that 53.7% of the patients showing TLS localized in the tumoral area (IT) were disease free at 60 months versus only 23.5% of patients whose tumors did not display TLS in the tumor core (log-rank test P = 0.008)
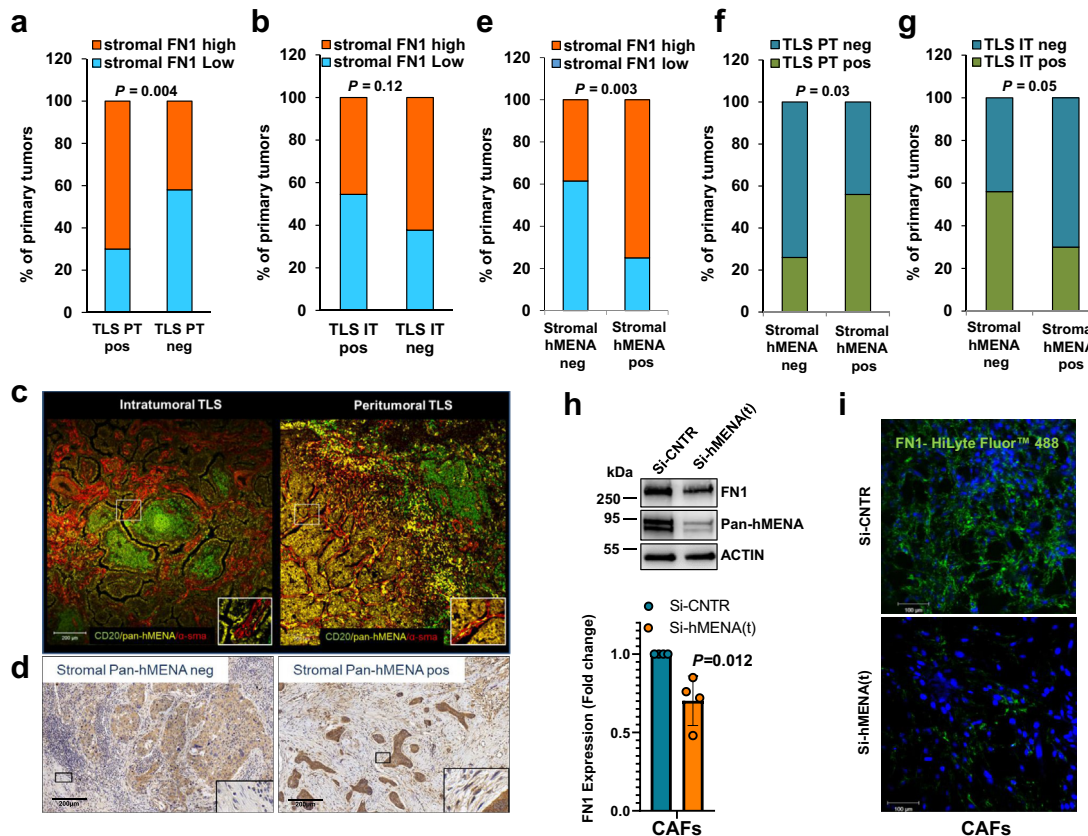
Fig. 4: NSCLC primary tumors with high level of stromal fibronectin display TLS localized in the peritumoral region (PT) and express stromal hMENA(t). a and b. Histograms relative to IHC of 94 node-negative NSCLC tissues showed that high stromal FN1 level associated with TLS PT (a) but not with TLS IT (b). P value was estimated with Fisher Exact test. **c.** Representative images of multiplex immunofluorescence labeling of two NSCLC cases showing TLS IT (CD20 green) and α-SMA positive stromal cells (red) negative for pan-hMENA staining (yellow) (left) or TLS PT with stromal cells both positive for hMENA staining (right) and α-SMA. Magnification 10×. Zooms of stromal area are indicated by white squares. **d.** Immunohistochemistry of consecutive sections of representative NSCLC cases with pan-hMENA negative or pan-hMENA positive stromal cells. **e–g.** Histograms relative to IHC characterization of 54 node-negative NSCLC tissues showed that stromal pan-hMENA positivity is associated with high stromal FN1 level (e), TLS PT positive (f) and TLS IT negative (g). P value was estimated with Fisher Exact test. **h.** Representative WB analysis of FN1 expression in CAF #377 transfected with control (Si-CNTR), and hMENA(t) pool siRNAs (Si-hMENA(t)) (upper panel). Densitometrically quantified data, represented as fold change of FN1/ACTIN ratio with respect to control (Si-CNTR) set as 1 (lower panel). Data are reported as the mean ± SD of 4 different CAF population (#358; #361; #376; #377). P value was calculated by paired 2-tailed Student's t test. **i.** Representative images of immunofluorescence of fibronectin fibrils (FN-488) in CAFs of patient #361, transfected with non-targeting control (CNTR) and hMENA(t) siRNAs. Nuclei were stained with 4′,6-diamidino-2-phenylindole (DAPI). Magnification 20×. Scale bar: 50 μm.

(Fig. 2b). Similar results were obtained with OS (Fig. 2c). No significant association was found between TLS and patient survival when only peritumoral TLS were considered in the analysis, even if Kaplan–Meier curves showed an opposite trend respect to TLS IT, with only 32% of 45 patients disease free at 60 months when TLS are PT with respect to 41.1% of 47 patients with no TLS PT (Fig. 2e and f). In this cohort of patients, TLS presence did not associate significantly with the probability of NSCLC patient survival (Supplementary Figure S7a), suggesting that TLS localization is a more precise prognostic indicator than their mere presence or absence in this subset of patients.

Differently, when we analyzed the CD3+ T lymphocytes distribution pattern of infiltration among the tissues analyzed we found that 64 cases display T cells present within the tumor nests whereas in the other 25 cases we did not found CD3+ T cells within the tumor nests (absent), even though they could be present in the tumor stroma. The absence of CD3+ T cells within the tumor nests was associated with DFS, but not with OS of the patients and proved significant only on univariate

analysis (Supplementary Tables S2 and S3). Finally, hMENA[11a] expression does not associate with the distribution of CD3+ T lymphocytes, suggesting that this isoform may influence the TLS organization rather that immune cell infiltration.

TLS localized within the tumor core are associated with switched memory intratumoral B cells

Given the emerging evidences indicating a prominent role of B cells in antitumor immunity,[7,46] we have analyzed B cell phenotype in peripheral blood (P), in non-tumoral tissue adjacent to the tumor site (N), and in the tumor site (T) of 8 patients with NSCLC whose primary tumors were positive (IT[+], n = 4) or negative (IT^{−}, n = 4) for the presence of TLS IT (Supplementary Table S4). As expected, TLS IT^{+} cases show an enrichment in B cells (CD19^{+}) in the tumor sites with respect to TLS IT^{−} cases (Fig. 3a left panel and Fig. 3b). In patients with TLS IT^{+}, the percentage of transitional (CD24^{+}CD38^{+}) and naïve (CD27^{−}IgD^{+}) B cells is reduced in the tissues with respect to the periphery (Fig. 3c and d, respectively), where we observed a significant lower percentage of naïve B cells in the IT^{+} with respect to the IT^{−} cases (Fig. 3d, right panel). Differently, the percentage of memory B cells (CD27^{+}) progressively increased from the periphery to the adjacent normal and to the tumor tissue in both patients with IT^{+} and IT^{−} (Fig. 3a right panel and Fig. 3e, left panel), while in the periphery, IT[+] cases showed a higher percentage of memory B cells with respect to the IT negative cases (Fig. 3e, right panel). Looking at the memory subsets, we observed that the unswitched memory B cells (CD27^{+}IgD^{+}) are significantly less frequent in the tissue site with respect to the periphery in the patients with TLS IT^{+} (Fig. 3f). The frequency of switched memory cells (CD27^{+}IgD^{−}) is significantly higher in TLS IT^{+} than TLS IT^{−} tissues (Fig. 3g, right panel). Moreover, in the TLS IT^{+} the switched memory cells are more represented in tissues compared to the periphery (Fig. 3g, left panel). This modulation is not evident in the TLS IT negative cases, suggesting that the presence of TLS IT is associated with the maturation of B cells in the tumor tissue, which may act as antigen presenting cells able to activate T cells and as tumor-antigen specific effectors supporting the generation of an integrated immune response of tumor-specific T cells and antibody producing B cells, in line with recent data in renal cancer.[12]

Intratumoral TLS associate with low stromal FN1 and paucity of hMENA positive CAFs

Distinct CAF populations have been reported associated with T cell exclusion in NSCLC[18] and FN1 belongs to the signature ECM-myCAF subtype.[14] The staining of FN1 in the tissues analyzed for TLS (representative cases are reported in Fig. 1d and e) revealed that FN1 level in the stroma strongly correlates with peritumoral but not with intratumoral TLS localization (Fig. 4a and b), suggesting

that a stroma enriched in a dense extracellular FN1 compromises the organization of TLS into the tumor core. Since FN1 is mainly produced by CAFs,[47,48] we thus looked at the expression of hMENA/hMENAΔv6 by pan-hMENA staining (hMENA(t)), in stromal cells morphologically resembling CAFs. Pan-hMENA staining was positive in the 50% of the 54 primary NSCLC cases as evaluated by conventional IHC (Fig. 4d) and confirmed in selected cases by for multiplex immunofluorescence (Fig. 4c). To confirm that stromal cells hMENA(t) positive are CAF we stained consecutive sections with pan-hMENA, α–SMA and FAP (Supplementary Figure S1a for a representative case of NSCLC with peritumoral TLS). Notably, we found that hMENA/hMENAΔv6 expression in the tumor stroma significantly correlates with high stromal FN1 (Fisher exact test P = 0.003, Fig. 4e) and these cases more frequently show TLS localized at the peritumoral region (PT, Fisher exact test P = 0.03, Fig. 4f). On the other hand, lack of stromal hMENA(t) expression correlates with TLS mainly organized in the tumor area (IT, Fisher exact test P = 0.05, Fig. 4g), suggesting that hMENA(t) positive CAFs might impede the organization of TLS within the tumor core.

Finally, multivariate analysis showed that the two variables, hMENA[11a] on tumor cells and pan-hMENA reactivity on stromal cells, were predictors of TLS presence in the tumor area (Supplementary Table S5). This analysis identified the pattern of hMENA isoform expression in tumor cells and CAFs as a determinant of ECM composition and TLS localization in early N0 patients with NSCLC.

Based on these clinico-pathological results, we then moved to highlight the role of hMENA/hMENAΔv6 in FN1 production and fibrillogenesis. We isolated CAFs from primary tumors of patients with NSCLC undergoing curative surgery (Supplementary Table S6). CAFs were extensively characterized as reported in materials and methods and in Supplementary Figure S1. CAFs express the hMENA/hMENAΔv6 isoforms along with CAF markers such as α-Smooth Muscle Actin (α-SMA, ACTA2 gene), Platelet-Derived Growth Factor receptor B (PDGFrB), Fibroblast Activated Protein (FAP), Podoplanin (PDPL) and Integrin β1 (ITGB1) and never express the epithelial markers EPCAM (Supplementary Figure S1b) and hMENA[11a].[26] Of interest, we found that the depletion of hMENA/hMENAΔv6 (hMENA(t)) in CAFs determines a reduction of FN1 expression and fibrillogenesis (Fig. 4h and i).

In CAFs, hMENA/hMENAΔv6 influence the expression and signaling of LTβR and the secretion of CXCL13. In tumor cells the 'epithelial' hMENA[11a] affects CXCL13 production by T$_{RM}$ cells

TLS deriving plasma cells disseminate into the tumor tissue along FAP negative fibroblastic tracks in renal cancer.[12] Furthermore, the development of TLS in

murine melanoma has been reported to be orchestrated by a subtype of FAP negative CAFs and their expansion promoted by the signaling of LTβR.[13] Notably, we recently demonstrated that the mesenchymal hMENA/hMENAΔv6 isoforms correlate with FAP expression in CAFs and play a crucial role in the pro-tumoral cancer cell/CAF crosstalk.[26] Herein, we evaluated whether hMENA/hMENAΔv6 isoform expression may impact LTβR signaling in CAFs. We found that CAFs express different levels of LTβR and that the depletion of hMENA/hMENAΔv6 (hMENA(t)) induces an increase of LTβR expression level (Fig. 5a).

Engaging of LTβR by its ligand LIGHT induces the activation of the canonical or non-canonical NF-kB pathway which could be revealed by the phosphorylation status of RelA (p65) or by the quantification of the ratio between the active p52 N-terminal half of the processed inactive p100 protein.[49] When we treated CAFs with LIGHT we observed a moderate increase in the phosphorylation of p65 and in the p52/p100 ratio that became highly significant after the hMENA(t) depletion (Fig. 5b). Consistently, the transfection of normal lung fibroblasts (IMR-90) with the hMENAΔv6 'mesenchymal' isoform hampered the LIGHT–mediated increase in the p65 phosphorylation and p52/p100 ratio (Supplementary Figure S8a). Considering that once activated the LTβR induces the secretion of CXCL13, we evaluated whether the hMENA(t) depletion in CAFs affected CXCL13 production. We found a significant increase of CXCL13 secretion in the conditioned medium of hMENA(t) depleted CAFs (Fig. 5c) and we observed that hMENAΔv6 transfection in IMR-90 reduced CXCL13 production (Supplementary Figure S8b). These data point to an inhibitory role of hMENA/hMENAΔv6 in LTβR signaling activation and CXCL13 production in NSCLC CAFs.

As TLS induction has been previously linked to CXCL13 production by T_{RM}, our hypothesis was that the secretome of hMENA[11a] tumor cells could influence the production of CXCL13 by T_{RM}. To test this, we analyzed the secretome of tumor cells, comparing those silenced or not for hMENA[11a] and untreated or treated with LIGHT. We investigated a panel of chemokines and cytokines and found a complex profile of cytokine/chemokine production across all experimental conditions. Expressing values as fold increase relative to the baseline, which was the conditioned media (CM) from non-hMENA[11a] silenced cells (Si-CNTR) in the absence of LIGHT, we observed up-regulation of both pro- and anti-inflammatory factors, with the exception of MIF and CCL25 that were down-regulated (Supplementary Figure S9).

We then treated tumor infiltrating lymphocytes, isolated from primary tumors of 8 patients with NSCLC (Supplementary Table S4), with the CM of tumor cells silenced or not for hMENA[11a]. As shown in Fig. 5d, the treatment with the CM of hMENA[11a] silenced H1650 cells significantly reduced the percentage of intratumoral CD8^{+} and CD4^{+} T_{RM} cells (CD103^{+}, an integrin binding E-Cadherin on tumor cells, and CD69^{+}) expressing CXCL13, compared to T_{RM} cells exposed to CM of control H1650 cells (Fig. 5d).

These data suggest that the expression of hMENA[11a] not only affects LTβR expression in tumor cells, but also modulates secreted proteins favoring CXCL13 production by T_{RM} cells and, thus potentially contributing to TLS formation.

hMENA11a[high]/hMENAΔv6[low]/FN1^{low} lung cancer cases display the gene expression signatures of TLS and low immunosuppressive ECM-myCAF signature

To validate our experimental data and the data obtained in our patient cohort exhibiting that hMENA[11a] expression is related to low stromal FN1 and intratumoral TLS localization, whereas high CAF expression of hMENA/hMENAΔv6 is inversely correlated with intratumoral TLS, we investigated these findings in early and advanced stage patients from LUSC and LUAD datasets from TCGA.[50] Firstly, by integrating the percentage of splicing events[34] and the expression levels of the known splice variants, we identified the patients showing expression for hMENAΔv6 variant and patients showing expression of hMENA[11a] variant. Moreover, we investigated the expression levels of FN1 gene in the group of patients showing expression for hMENAΔv6 variant (Supplementary Figure S10 for patients with early stage NSCLC). In line with our previous results[24] we found that early stage patients with hMENAΔv6[high] and FN1^{high} had a shorter OS (Fig. 6a) compared to the patients with hMENA11a[high]/hMENAΔv6[low] (thereafter named hMENA11a[high]) (log-rank test P = 0.0056). These two groups of patients do not show any enrichment of mutations (Supplementary Table 7) and, in accordance to the data of the experimental cohort, the hMENA[11a] has a prognostic relevance in the early but not in advanced patients with NSCLC (Supplementary Figure S11). Interestingly, when we stratified patients considering two different signatures of TLS[12,36] in combination with the signature of immunosuppressive ECM-myCAF,[14] we found that patients with hMENA11a[high] were enriched for both TLS signatures along with ECM-myCAF low signature (Fisher's exact test P = 0.0001 for the TLS classic signature, and P = 0.001 for the TLS Meylan signature) (Fig. 6b and c). The validation in the TCGA dataset strongly support our experimental results and data in NSCLC tissues.

hMENA splicing affects response to ICB in tumors where TLS are related to an anti-tumor immune response

To translate our experimental and clinical data in a setting of ICB treated patients with NSCLC we analyzed the 770 genes of the IO 360 panel (Nanostring) customized with probes for hMENA[11a], hMENA and
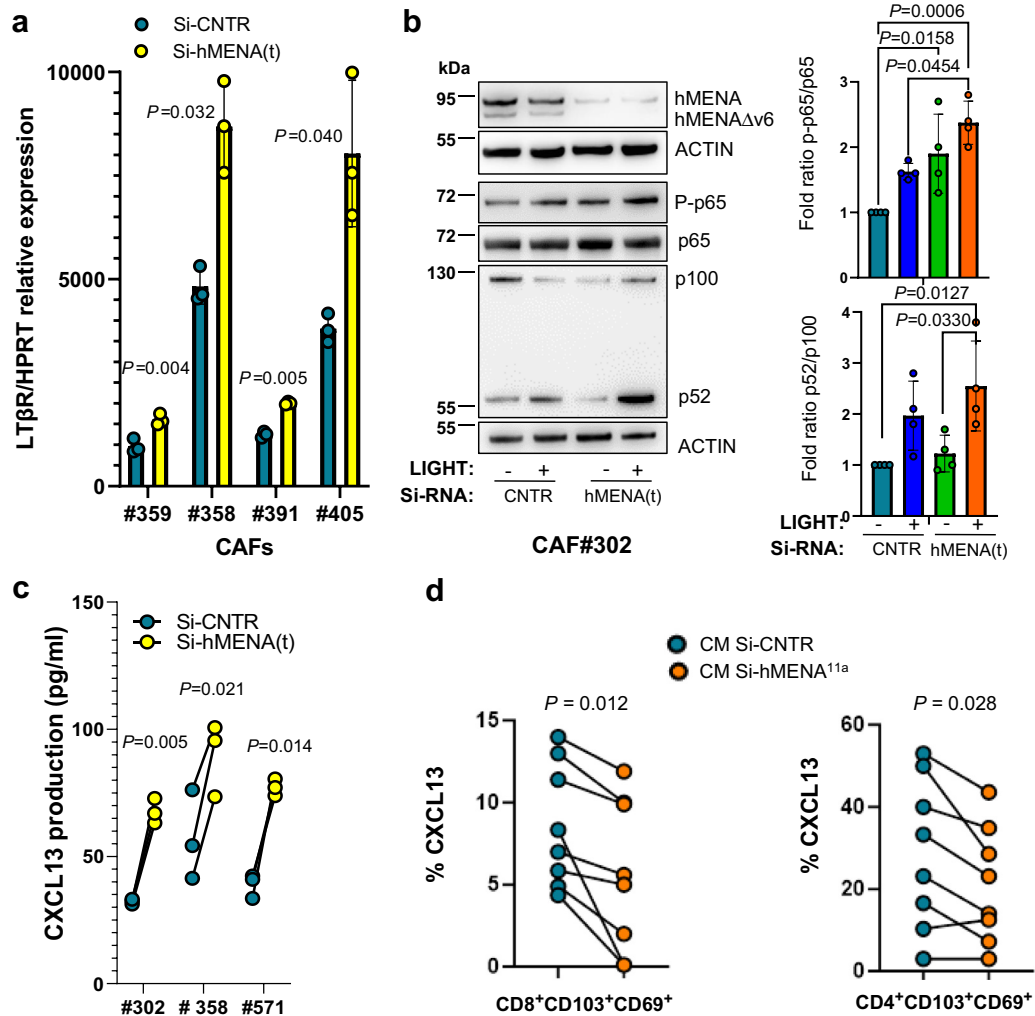
Fig. 5: hMENA/hMENAΔv6 influences the expression and signaling of LTβR and the secretion of CXCL13 in CAFs. The 'epithelial' hMENA[11a] isoform in tumor cells affects CXCL13 production by T_RM cells. a. qRT-PCR analysis of LTβR mRNA expression in the CAFs obtained from four different patients with NSCLC (#359, #358, #391, #405), transfected with control (Si-CNTR), and hMENA(t) pool siRNAs (Si-hMENA(t)). Data reported are the mean of technical triplicates. P value of paired 2-tailed Student's t test is reported. b. Representative WB analysis with the indicated Abs of protein extracts from CAF #302 transfected with non-targeting siRNA (Si-CNTR) or with hMENA(t) siRNA, untreated or treated with 50 ng/mL of LIGHT for 24 h. Fold change of P-p65/p65 and of p52/p100 staining intensity (right). Data reported are the mean of 4 different experiments ± SD. Adjusted P values of One-way ANOVA followed by Tukey's multiple comparisons procedures are reported when significant. c. CXCL13 production evaluated by ELISA assay of CAFs derived from three different patients (#302; #358; #571) transfected with non-targeting siRNA (Si-CNTR) or with hMENA(t) siRNA. Data reported are the mean of technical triplicates of pg/mL normalized for total protein content in three biological replicates. P value of paired two tailed t test, is reported d. Percentage of CXCL13 chemokine, evaluated by multiparametric flow cytometry, in ex-vivo TILs isolated from eight patients with NSCLC, after culture (24 h) with CM from H1650 tumor cells silenced for hMENA[11a] (Si-hMENA[11a]), or control (Si-CNTR). Results within CD8+ T_RM (CD103+CD69+, left panel) or CD4+ T_RM (CD103+CD69+, right panel) are shown. Statistical significance was determined using non-parametric Wilcoxon rank test.

hMENAΔv6 variants, FN1 and LTβR in the tissue samples of 12 ICB treated patients with NSCLC (clinico-pathological characteristics in Supplementary Table S8 and top mutated genes detected by Whole-Exome Sequencing Analysis in Supplementary Figure S12). The patients were classified as poor responders, in case of disease progression at 3 months of treatment, or good responders in the absence of progression after 10 months.

For each of the custom probes we have evaluated a cut-off of the normalized value based on the ROC curve designed on the response to therapy. The relative variables were considered high or low on the basis of the respective cut-off. Data reported in Fig. 6d (normalized
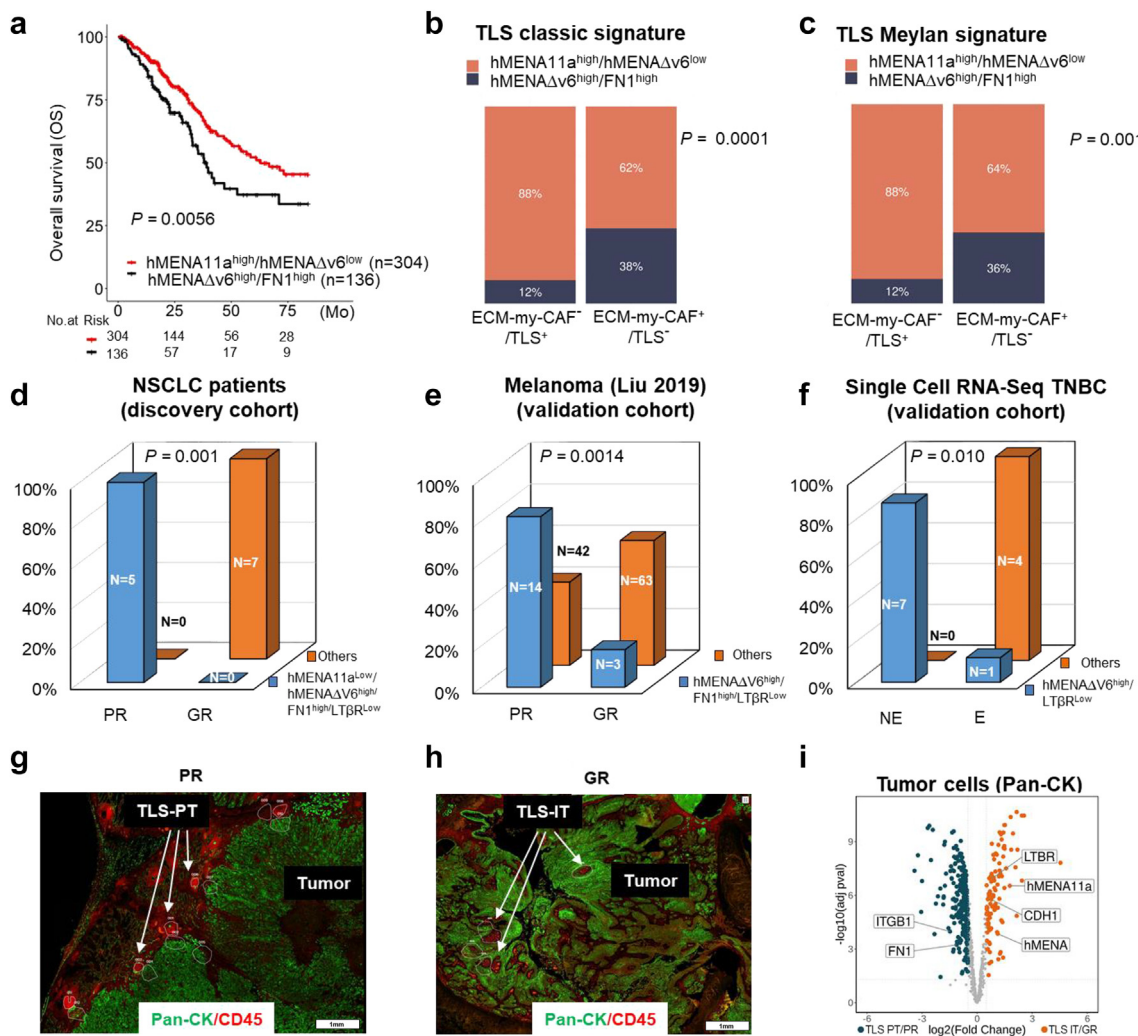
Fig. 6: hMENA11a^high^/hMENAΔv6^low^ favors OS in TGCA patients with lung cancer and associate with TLS and low immunosuppressive ECM-myCAF signatures. The pattern of hMENA isoforms impacts ICB response. a. OS curves in early stages patients with LUNG cancer (LUSC and LUAD) from The Cancer Genome Atlas (TCGA). Patients were stratified into two groups, hMENA11a^high^/hMENAΔv6^low^ and hMENAΔv6^high^/FN1^high^, on the basis of the specific percent spliced-in (PSI) values for exon 6 and 11a and the expression levels for FN1 gene and 11a isoform. Statistical significance was calculated by using the log-rank test. P value is shown. **b and c.** Barplots showing the percentage of hMENA11a^high^/hMENAΔv6^low^ and hMENAΔv6^high^/FN1^high^ cases defined as in **a**, stratified according to the classic cytokine-based TLS signature (b) and the Ig-enriched TLS signature (Meylan, c) in combination with the signature of immunosuppressive ECM-myCAF (CAF). The percentage of hMENA11a^high^/hMENAΔv6^low^ and hMENAΔv6^high^/FN1^high^ cases in each group and P values are shown. **d.** Nanostring analysis of NSCLC tissues from 12 ICB treated patients with high or low levels of hMENA,[11a] hMENAΔv6, FN1 and LTβR indicating that tumor tissues of all the poor responder patients (PR) are hMENA11a^low^, hMENAΔv6^high^, FN1^high^ and LTβR^low^. **e.** Proportions of patients with melanoma with response to ICB treatment (GR) or with poor response to treatment (PR), stratified by hMENAΔv6 isoform, FN1 and LTβR expression level. **f.** Proportions of patients with TNBC with response to anti-PD1 treatment (i.e., T cell expanded, 'E') or with non-response to treatment (i.e., T cell non-expanded, 'NE'), stratified by hMENAΔv6 splicing and LTβR expression level. **b–f.** All P values were estimated using Fisher Exact Test. **d–f.** N = Number of Patients. **g and h.** Representative images of NSCLC tissues from PR patient with TLS PT and GR patient with TLS IT, morphologically defined by Pan-CK (green, tumor cells) and CD45 (red, immune cells) obtained by GeoMx DSP platform. **i.** Volcano plots showing differentially expressed genes (q < 0.05, n = 581) in TLS PT/PR versus TLS IT/GR patients in their tumor cells. Reported are the negative log10-transformed adjusted P values plotted against the log2 fold changes. Dots represent individual genes. Genes of interest are indicated.

expression of Nanostring transcriptome data relative to the custom probes are reported in Supplementary Table S9), indicate that the tumors expressing low hMENA[11a], high hMENA/hMENAΔv6, low LTβR and high FN1, identify the poor responder patients supporting the results we have reported in our cohort of

treatment-naïve patients with NSCLC. These findings highlight the role of hMENA isoform expression pattern in participating in anti-tumor immunity and patient survival and suggest that the above signature may discriminate the response of patients with NSCLC to ICB therapy.

To decipher the determinants of TLS localization in patients with NSCLC, we spatially profiled, in 2 tumor tissues the expression of 1800 transcripts complemented with custom probes for the three hMENA splice variants by NanoString GeoMx Cancer Genome Atlas Assay. Tumor sections were stained with markers for immune (CD45), stromal (α-SMA) and epithelial (Pan-CK) compartments to profile RNA from the tumor cells (Pan-CK+), fibroblasts and TLS (CD45+). As expected, the hMENA[11a] isoform is prevalent in the tumor cells, whereas hMENAΔv6 is mainly expressed in the stromal cells morphologically resembling CAFs (Supplementary Figure S13). We then applied GeoMx DSP analysis to tissues from a good responder patient with TLS IT and a poor responder with TLS PT (Fig. 6g and h). The expression of multiple cytokeratin genes (Pan-CK) in the tumor areas evidenced the reliability of the data. A total of 17 region of interest (ROI) from tumor cell areas were analyzed. The analysis revealed that hMENA[11a] and LTβR are significantly up-regulated in the tumoral compartment of the GR patient with TLS-IT, whereas FN1 is up-regulated in the tumor cells of PR patient with TLS-PT (Fig. 6i and Supplementary Table S10). These data extend at spatial level the role of hMENA[11a] in TLS localization and in response to ICB.

To confirm the role of hMENA isoforms as predictors of ICB response identified in our experimental cohort, we then interrogated RNA-Seq datasets of ICB treated patients with melanoma, a tumor where TLS presence is related to antitumor immune response and sensitivity to ICB.[10] Among the available datasets we focused on the largest (122 patients with melanoma) by Liu et al.[40] Firstly, we identified the three hMENA isoforms from bulk RNA-Seq (see methods) and then grouped the patients by clinical benefit (complete response + partial response + stable disease versus progressive disease). The results evidenced that a signature based on high hMENAΔv6, high FN1 and low LTβR identifies patients with melanoma resistant to the ICB treatment (Fig. 6e) (Fisher's exact test P = 0.0014).

Considering our experimental data indicating that expression of hMENAΔv6 in CAFs affects LTβR expression (Fig. 5a), we also exploited a single cell RNA-Seq data of triple-negative breast cancer (TNBC), a subtype close related to a mesenchymal phenotype, treated with anti-PD-1.[51] Considering the exon 6 skipping to identify the patients with fibroblasts hMENAΔv6[high], we evidenced that 7 out of 8 patients with high hMENAΔv6 and low LTβR were not responding to

anti-PD-1 treatment (Fig. 6f) (Fisher's exact test P = 0.01).

All together, these findings highlight the role that hMENA splicing may exert as orchestrator of a TIME, influencing ICB response where TLS presence is related to an anti-tumor immune response.

Discussion

Herein, we report unexplored cellular and molecular mechanisms driven by the actin regulator hMENA in both tumor cells and CAFs and demonstrate the role of hMENA isoforms in TLS organization and localization in patients with NSCLC, with an impact on patient prognosis and likely response to ICB therapy.

To highlight whether hMENA and its isoforms may orchestrate different tumor immune microenvironments, we focused on TLS, stromal cells and ECM, firstly analyzing a cohort of treatment-naive lymph node negative patients, who are still lacking of criteria for clinical management. Given the established role of the extracellular matrix, including FN1, in the localization and interactions of immune cells, and its likely involvement in the formation of tertiary lymphoid structures (TLS), we hypothesized that investigating FN1 could be crucial in understanding the ECM components in the context of TLS. We found that hMENA[11a] high expression in tumor cells correlates with low level of stromal FN1, as we previously reported[24] and, as novelty, we evidenced that hMENA[11a] highly expressing tumors have TLS localized in the tumor core. Notably, we provide evidence that TLS localization within the tumor core (IT) is related to both a longer DFS and OS, whereas peritumoral TLS localization (PT) is more frequent in patients with a shorter survival and significantly associated with higher tumor grade (Fig. 2). These data point on the importance of the functional significance of TLS localization in controlling tumor progression and likely response to immunotherapy. While the precise mechanism linking the expression of hMENA[11a] in tumor cells to intratumoral TLS is yet to be completely understood, our data strongly suggest that hMENA[11a] induces the expression of LTβR, as illustrated in Fig. 1a and b. This implies that the association between hMENA[11a] and TLS may be attributed to the modulation of this crucial receptor, potentially influencing TLS development.[52] Furthermore, it can be argued that the presence of hMENA[11a] expressing tumor cells, by impacting FN1[24] may in turn reduce matrix stiffness[53] and favor immune cell infiltration. These findings are also supported by RNA-Seq data where we found an increase in the expression of FN1 and a decrease in the expression of LTβR when hMENA[11a] isoform is specifically silenced (Fig. 1a). In line with these results, recent data indicate that hMENA regulates actin-nuclear lamina interaction and chromatin organization at the nuclear periphery and immune response-

related genes.[25] Notably, in agreement with our previous results,[24] hMENA regulates the expression of the ECM component FN1.[25]

That hMENA[11a] participates in orchestrating a TLS-related TIME subtype is also supported by the identification of a paracrine signal generated by hMENA[11a] expressing tumor cells and acting on T_{RM} cells. While the specific immune-related molecules involved remain unknown, our data clearly demonstrates that the depletion of hMENA[11a] in tumor cells results in significant alterations in the relative amounts and quality of secreted cytokines and chemokines, ultimately leading to a reduction in CXCL13-producing T_{RM} cells (Fig. 5d). These findings support a role for hMENA[11a] expression in shaping a favorable TME characterized by the infiltration of CXCL13-producing T cells. This, in turn, is associated with the organization of TLS, an event previously reported and linked to a clinical response to anti-PD-1 treatment in NSCLC.[27]

These findings also sustain our data that patients with TLS localized in the tumor site show a higher percentage of switched memory B cells and a lower percentage of naïve B cells both in the periphery and in the tumor site (Fig. 3d–g), which argues for an anti-tumor specific B cell response, as recently demonstrated by Meylan and coauthors in renal cell cancer.[12] Noteworthy, since hMENA and hMENA[11a] have been identified from the antibody response of a long surviving breast cancer patient[39] we could envision that hMENA[11a] related signaling contributes to a TLS-TIME, which favors a tumor specific B and T immune response, that will be further explored.

CAF subtypes are involved in immune cell exclusion and immune suppression[18] and, of relevance, the IgG producing plasma cells disseminate into the tumor along tracks of specific fibroblasts expressing the MCP-counter signature,[12] which does not include *FAP* gene. Of relevance, other Authors found that only FAP negative CAFs promote the development of TLS in murine melanoma.[13] This is consistent with our previous findings that depletion of hMENA/hMENAΔv6, which we have previously reported to be correlated with FAP expression,[26] leads to an increase in LTβR expression (Fig. 5a). Notably, the hMENA silencing in CAFs engendered the downstream NF-kB activation and CXCL13 secretion, whereas the hMENAΔv6 transfection in normal lung fibroblasts reduces the canonical and non-canonical NF-kB signalling pathway as well as the CXCL13 secretion (Supplementary Figure S8a and b). The immune suppressive role of hMENA in CAFs is also supported by data that hMENA (*ENAH*) is one of the genes highly expressed in the immunosuppressive FAP positive ECM-myCAF subtype, involved in primary immunotherapy resistance[14] and by our previous results that hMENA in CAFs is fundamental in regulating the immunosuppressive GAS6-AXL axis.[26] Our experimental findings, that hMENA/hMENAΔv6 in NSCLC derived CAFs is correlated to FN1 expression and fibrillogenesis (Fig. 4h) are sustained by *in vivo* results revealing that hMENA/hMENAΔv6 isoforms are highly expressed in CAFs of tumor tissues with high level of stromal FN1 and TLS preferentially localized in the peritumoral region. The data that the dense expression of FN1 may act as barrier in intratumoral TLS localization are in agreement with the reduced capability of T cells to enter the tumor nests when FN1 is highly expressed[17] and with the immune suppressive stromal checkpoint function of FN1-Immunoglobulin-like transcript 3 (ILT3) interaction that may represent a substantial barrier to anti-tumor immune response and immunotherapy efficacy.[54]

The validation of our data in a TCGA dataset of early NSLCL tissues (stage 1–2) confirm and extend at the level of specific exon expression our previous data,[24] showing that patients hMENAΔv6[high] and FN1^{high} have a shorter OS with respect to patients expressing hMENA11a[high] on their primary tumors. Notably, TCGA dataset revealed that hMENA11a[high] tumors display a low signature of immunosuppressive ECM-myCAF[14] and high TLS signature as evaluated considering the classic, 12-cytokines,[36] as well as the Meylan, Ig-enriched 29-gene signature.[12] On the other hand, the hMENAΔv6[high]/FN1^{high} tumors associate with low TLS signatures (Fig. 6b and c).

Only few factors have been reported as able to reciprocally reprogram the tumor/stroma communication. As novelty, in support of our previous data that the actin cytoskeleton regulatory protein hMENA orchestrates the pro-tumor communication between tumor cells and CAFs by GAS6-AXL pathway,[26] herein we demonstrate that the epithelial-associated hMENA[11a] favors a tumoral secretome which not only restrains FN1 production,[24] but influences B cell organization in TLS and their intratumoral localization. This study likely provides an explanation for the better prognosis we have previously and herein reported of patients with NSCLC tumors expressing hMENA[11a], with respect to tumors expressing low hMENA[11a] and high hMENAΔv6 isoform. We envisage for a relevant contribution of the hMENA[11a]-related signaling and secretome in the maintenance and expansion of a long term tumor immunity. This is strongly supported by the transcriptomic analysis of NSCLC tissues from 12 ICB treated patients, where a signature based on the pattern of hMENA isoforms, FN1 and LTβR expression may discriminate patients with NSCLC responding or not-responding to ICB (Fig. 6d). Interestingly, selected cases spatially resolved show an enrichment of hMENA[11a] and LTβR in the tumor cells of good responder patients with TLS IT and of FN1 in the poor responder patients with TLS PT, thus highlighting by digital spatial profiling the IHC data linking hMENA[11a] and FN1 to the TLS localization.

The validation of NSCLC data in melanoma and in TNBC reinforce the role of hMENA isoform pattern of

expression and TLS as predictors of ICB efficacy, to be further explored in first line ICB-treated patients or in neo-adjuvant setting.

References

1 Chaft JE, Shyr Y, Sepesi B, Forde PM. Preoperative and post-operative systemic therapy for operable non-small-cell lung cancer. *J Clin Oncol.* 2022;40(6):546–555.

2 Binnewies M, Roberts EW, Kersten K, et al. Understanding the tumor immune microenvironment (TIME) for effective therapy. *Nat Med.* 2018;24(5):541–550.

3 Reck M, Rodríguez-Abreu D, Robinson AG, et al. Updated analysis of KEYNOTE-024: pembrolizumab versus platinum-based chemotherapy for advanced non-small-cell lung cancer with PD-L1 tumor proportion score of 50% or greater. *J Clin Oncol.* 2019;37(7):537–546.

4 Martinez P, Peters S, Stammers T, Soria JC. Immunotherapy for the first-line treatment of patients with metastatic non-small cell lung cancer. *Clin Cancer Res.* 2019;25(9):2691–2698.

5 Galon J, Bruni D. Approaches to treat immune hot, altered and cold tumours with combination immunotherapies. *Nat Rev Drug Discov.* 2019;18(3):197–218.

6 Sautès-Fridman C, Petitprez F, Calderaro J, Fridman WH. Tertiary lymphoid structures in the era of cancer immunotherapy. *Nat Rev Cancer.* 2019;19(6):307–325.

7 Germain C, Gnjatic S, Tamzalit F, et al. Presence of B cells in tertiary lymphoid structures is associated with a protective immunity in patients with lung cancer. *Am J Respir Crit Care Med.* 2014;189(7):832–844.

8 Petitprez F, de Reyniès A, Keung EZ, et al. B cells are associated with survival and immunotherapy response in sarcoma. *Nature.* 2020;577(7791):556–560.

9 Helmink BA, Reddy SM, Gao J, et al. B cells and tertiary lymphoid structures promote immunotherapy response. *Nature.* 2020;577(7791):549–555.

10 Cabrita R, Lauss M, Sanna A, et al. Tertiary lymphoid structures improve immunotherapy and survival in melanoma. *Nature.* 2020;577(7791):561–565.

11 Patil NS, Nabet BY, Müller S, et al. Intratumoral plasma cells predict outcomes to PD-L1 blockade in non-small cell lung cancer. *Cancer Cell.* 2022;40(3):289–300.e4.

12 Meylan M, Petitprez F, Becht E, et al. Tertiary lymphoid structures generate and propagate anti-tumor antibody-producing plasma cells in renal cell cancer. *Immunity.* 2022;55(3):527–541.e5.

13 Rodriguez AB, Peske JD, Woods AN, et al. Immune mechanisms orchestrate tertiary lymphoid structures in tumors via cancer-associated fibroblasts. *Cell Rep.* 2021;36(3):109422.

14 Kieffer Y, Hocine HR, Gentric G, et al. Single-cell analysis reveals fibroblast clusters linked to immunotherapy resistance in cancer. *Cancer Discov.* 2020;10(9):1330–1351.

15 Hanley CJ, Waise S, Ellis MJ, et al. Single-cell analysis reveals prognostic fibroblast subpopulations linked to molecular and immunological subtypes of lung cancer. *Nat Commun.* 2023;14(1):387.

16 Nicolas-Boluda A, Vaquero J, Vimeux L, et al. Tumor stiffening reversion through collagen crosslinking inhibition improves T cell migration and anti-PD-1 treatment. *Elife.* 2021;10:e58688.

17 Salmon H, Franciszkiewicz K, Damotte D, et al. Matrix architecture defines the preferential localization and migration of T cells into the stroma of human lung tumors. *J Clin Invest.* 2012;122(3):899–910.

18 Grout JA, Sirven P, Leader AM, et al. Spatial positioning and matrix programs of cancer-associated fibroblasts promote T cell exclusion in human lung tumors. *Cancer Discov.* 2022;12(11):2606–2625.

19 Mhaidly R, Mechta-Grigoriou F. Role of cancer-associated fibroblast subpopulations in immune infiltration, as a new means of treatment in cancer. *Immunol Rev.* 2021;302(1):259–272.

20 Jenkins L, Jungwirth U, Avgustinova A, et al. Cancer-associated fibroblasts suppress CD8+ T cell infiltration and confer resistance to immune checkpoint blockade. *Cancer Res.* 2022;82(16):2904–2917.

21 Trono P, Sistigu A, Palermo B, Ciliberto G, Nisticò P. Mesenchymal traits at the convergence of tumor-intrinsic and -extrinsic mechanisms of resistance to immune checkpoint blockers. *Emerg Top Life Sci.* 2017;1(5):471–486.

22 Di Modugno F, Iapicca P, Boudreau A, et al. Splicing program of human MENA produces a previously undescribed isoform associated with invasive, mesenchymal-like breast tumors. *Proc Natl Acad Sci U S A.* 2012;109(47):19280–19285.

23 Melchionna R, Iapicca P, Di Modugno F, et al. The pattern of hMENA isoforms is regulated by TGF-beta 1 in pancreatic cancer and may predict patient outcome. *Oncoimmunology.* 2016;5(12):e1221556.

24 Di Modugno F, Spada S, Palermo B, et al. hMENA isoforms impact NSCLC patient outcome through fibronectin/β1 integrin axis. *Oncogene.* 2018;37(42):5605–5617.

25 Li Mow Chee F, Beernaert B, Griffith BGC, et al. Mena regulates nesprin-2 to control actin-nuclear lamina associations, trans-nuclear membrane signalling and gene expression. *Nat Commun.* 2023;14(1):1602.

26 Melchionna R, Spada S, Di Modugno F, et al. The actin modulator hMENA regulates GAS6-AXL axis and pro-tumor cancer/stromal cell cooperation. *EMBO Rep.* 2020;21(11):e50078.

27 Thommen DS, Koelzer VH, Herzig P, et al. A transcriptionally and functionally distinct PD-1. *Nat Med*. 2018;24(7):994–1004.

28 Workel HH, Lubbers JM, Arnold R, et al. A transcriptionally distinct CXCL13 + CD103 + CD8 + T-cell population is associated with B-cell recruitment and neoantigen load in human cancer. *Cancer Immunol Res*. 2019;7(5):784–796.

29 Shuster JJ. Median follow-up in clinical trials. *J Clin Oncol*. 1991;9(1):191–192.

30 Ewels PA, Peltzer A, Fillinger S, et al. The nf-core framework for community-curated bioinformatics pipelines. *Nat Biotechnol*. 2020;38(3):276–278.

31 McKenna A, Hanna M, Banks E, et al. The genome analysis toolkit: a MapReduce framework for analyzing next-generation DNA sequencing data. *Genome Res*. 2010;20(9):1297–1303.

32 Bria E, Di Modugno F, Sperduti I, et al. Prognostic impact of alternative splicing-derived hMENA isoforms in resected, node-negative, non-small-cell lung cancer. *Oncotarget*. 2014;5(22):11054–11063.

33 Vivian J, Rao AA, Nothaft FA, et al. Toil enables reproducible, open source, big biomedical data analyses. *Nat Biotechnol*. 2017;35(4):314–316.

34 Ryan M, Wong WC, Brown R, et al. TCGASpliceSeq a compendium of alternative mRNA splicing in cancer. *Nucleic Acids Res*. 2016;44(D1):D1018–D1022.

35 Liu J, Lichtenberg T, Hoadley KA, et al. An integrated TCGA pan-cancer clinical data resource to drive high-quality survival outcome analytics. *Cell*. 2018;173(2):400–416.e11.

36 Coppola D, Nebozhyn M, Khalil F, et al. Unique ectopic lymph node-like structures present in human primary colorectal carcinoma are identified by immune gene array profiling. *Am J Pathol*. 2011;179(1):37–45.

37 Trono P, Di Modugno F, Circo R, et al. hMENA(11a) contributes to HER3-mediated resistance to PI3K inhibitors in HER2-overexpressing breast cancer cells. *Oncogene*. 2016;35(7):887–896.

38 D'Antonio M, D'Onorio De Meo P, Pallocca M, et al. RAP: RNA-Seq analysis pipeline, a new cloud-based NGS web application. *BMC Genomics*. 2015;16:S3.

39 Di Modugno F, Bronzi G, Scanlan M, et al. Human mena protein, a serex-defined antigen overexpressed in breast cancer eliciting both humoral and CD8(+) T-cell immune response. *Int J Cancer*. 2004;109(6):909–918.

40 Liu D, Schilling B, Sucker A, et al. Integrative molecular and clinical modeling of clinical outcomes to PD1 blockade in patients with metastatic melanoma. *Nat Med*. 2019;25(12):1916–1927.

41 Patro R, Duggal G, Love MI, Irizarry RA, Kingsford C. Salmon provides fast and bias-aware quantification of transcript expression. *Nat Methods*. 2017;14(4):417–419.

42 Zheng GX, Terry JM, Belgrader P, et al. Massively parallel digital transcriptional profiling of single cells. *Nat Commun*. 2017;8:14049.

43 Dong K, Zhang C, Tian X, et al. Renal plasticity revealed through reversal of polycystic kidney disease in mice. *Nat Genet*. 2021;53(12):1649–1663.

44 Hui KPY, Ho JCW, Cheung MC, et al. SARS-CoV-2 Omicron variant replication in human bronchus and lung ex vivo. *Nature*. 2022;603(7902):715–720.

45 Nayar S, Campos J, Smith CG, et al. Immunofibroblasts are pivotal drivers of tertiary lymphoid structure formation and local pathology. *Proc Natl Acad Sci U S A*. 2019;116(27):13490–13497.

46 Sautès-Fridman C, Verneau J, Sun CM, et al. Tertiary Lymphoid Structures and B cells: clinical impact and therapeutic modulation in cancer. *Semin Immunol*. 2020;48:101406.

47 Barbazán J, Matic Vignjevic D. Cancer associated fibroblasts: is the force the path to the dark side? *Curr Opin Cell Biol*. 2019;56:71–79.

48 Erdogan B, Ao M, White LM, et al. Cancer-associated fibroblasts promote directional cancer cell migration by aligning fibronectin. *J Cell Biol*. 2017;216(11):3799–3816.

49 Pomerantz JL, Baltimore D. Two pathways to NF-kappaB. *Mol Cell*. 2002;10(4):693–695.

50 Network CGAR. Comprehensive molecular profiling of lung adenocarcinoma. *Nature*. 2014;511(7511):543–550.

51 Bassez A, Vos H, Van Dyck L, et al. A single-cell map of intra-tumoral changes during anti-PD1 treatment of patients with breast cancer. *Nat Med*. 2021;27(5):820–832.

52 Tang H, Zhu M, Qiao J, Fu YX. Lymphotoxin signalling in tertiary lymphoid structures and immunotherapy. *Cell Mol Immunol*. 2017;14(10):809–818.

53 Wang W, Taufalele PV, Millet M, et al. Matrix stiffness regulates tumor cell intravasation through expression and ESRP1-mediated alternative splicing of MENA. *Cell Rep*. 2023;42(4):112338.

54 Paavola KJ, Roda JM, Lin VY, et al. The fibronectin-ILT3 interaction functions as a stromal checkpoint that suppresses myeloid cells. *Cancer Immunol Res*. 2021;9(11):1283–1297.